Lab on a Chip

CRITICAL REVIEW

View Article Online
View Journal | View Issue

Cite this: *Lab Chip*, 2017, **17**, 11

Advancements in microfluidics for nanoparticle separation

Thoriq Salafi,[ab] Kerwin Kwek Zeming[b] and Yong Zhang*[ab]

Received 19th August 2016,
Accepted 26th October 2016

DOI: 10.1039/c6lc01045h

www.rsc.org/loc

Nanoparticles have been widely implemented for healthcare and nanoscience industrial applications. Thus, efficient and effective nanoparticle separation methods are essential for advancement in these fields. However, current technologies for separation, such as ultracentrifugation, electrophoresis, filtration, chromatography, and selective precipitation, are not continuous and require multiple preparation steps and a minimum sample volume. Microfluidics has offered a relatively simple, low-cost, and continuous particle separation approach, and has been well-established for micron-sized particle sorting. Here, we review the recent advances in nanoparticle separation using microfluidic devices, focusing on its techniques, its advantages over conventional methods, and its potential applications, as well as foreseeable challenges in the separation of synthetic nanoparticles and biological molecules, especially DNA, proteins, viruses, and exosomes.

Introduction

Nanoparticles have been widely employed for industrial applications spanning from photovoltaics,[1] supercapacitors,[2] cosmetics,[3] food,[4] and drug delivery,[5] to medical diagnostics[6] and therapy.[7] The sorting and separation of nanoparticles from heterogeneously sized mixtures are essential as nanoparticle synthesis procedures often result in a polydispersed size, and the physical and chemical properties of these nanoparticles depend on their size.[8,9] More importantly, high-performance nanoparticle sorting methods to filter nanoparticles from household and industrial waste are critical, as exposure to these nanoparticles introduces new hazards to health and the environment.[10,11] Improvement in nanoparticle separation methods is also important for the development of medical diagnostic tools, as biomolecules are often used as disease biomarkers, and the detection of viral particles is of great interest for viral diagnostics.[12,13] Moreover, recent research on nanometer-sized extracellular vesicles, such as exosomes, draws great interest for medical diagnostics and therapeutics.[14] The purification and separation of these extracellular vesicles from other molecules present in a

[a] *NUS Graduate School for Integrative Sciences and Engineering, Centre for Life Sciences (CeLS), National University of Singapore, 05-01 28 Medical Drive, 117456 Singapore. E-mail: biezy@nus.edu.sg*
[b] *Department of Biomedical Engineering, National University of Singapore, 9 Engineering Drive 1, Block EA #03-12, 117576 Singapore*

Thoriq Salafi

Thoriq Salafi earned his bachelor degree in Biomedical Engineering from the National University of Singapore (NUS). Currently, he is enrolled in a PhD and MBA double degree program at the NUS Graduate School for Integrative Sciences & Engineering (NGS) and NUS Business School. His current research focuses on microfluidic sorting and bioelectronics for medical diagnostics and commercialization.

Kerwin Kwek Zeming

Kerwin Kwek Zeming is a Postdoc Research Fellow at the Department of Biomedical Engineering, National University of Singapore (NUS). His PhD thesis investigates novel pillar shapes in deterministic lateral displacement microfluidic devices for the separation of key bio-particles, such as red blood cells and bacteria. His research interests include advances in nano/microfluidics for the detection of biological particles.

sample are one of the challenges to be overcome before further diagnostic steps can be performed.[15] There are several conventional techniques that have been commonly applied to perform these functions, including ultracentrifugation, electrophoresis, chromatography, filtration, size-selective precipitation, and solvent addition.[9,16] These techniques are proven to have high separation efficiency and reproducibility. However, they still have significant limitations, including the need for a minimum sample volume, multi-step preparation, and performance in batch mode. Additionally, each individual separation technique requires specific optimization for the separation of various nanoparticles, depending on sample properties, such as purity, density, solubility, hydrophobicity, solution conductivity, and particle isoelectric charge. As a result, the development of tools capable of addressing these drawbacks is needed to obtain more robust, versatile, and high-performance nanoparticle separation.

Recently, continuous particle separations with microfluidic technologies have been widely implemented due to their low cost, low sample volume, and minimal sample handling with precise control. Various microfluidic techniques have been explored extensively to separate micro-sized particles, such as blood cells,[17] spores,[18] parasites,[19] circulating tumor cells,[20] and bacteria.[21] Several review papers have also discussed microfluidics for microparticle and cell separation.[22–25] To separate submicron particles, nanofluidics has emerged as a suitable technique for separation. However, fabrication of nanofluidic devices increases complexity and requires expensive equipment.[26] Meanwhile, the advancement of microfluidics research has extended the separation resolution to reach the nano-regime, so as to perform nanoparticle purification and DNA isolation with superior efficiency compared to conventional nanoparticle separation methods. However, microfluidic techniques for nanoparticle separation have not been explored extensively, despite gaining momentum in recent years. This review gives an overview of traditional techniques to separate nanoparticles and explains the current development of nanoparticle separation methods using microfluidics, their advantages, applications, and foreseeable challenges for the separation of nanoparticles and biological molecules.

Yong Zhang

Yong Zhang is a Professor and Deputy Head of Research at the Department of Biomedical Engineering, National University of Singapore (NUS), and a senior member of NUS NanoCore Research Institute and NUS Graduate School for Integrative Sciences and Engineering (NGS). His current research interests include nanobiophotonics, nanomedicine, biomedical microdevices, and tissue engineering.

Conventional techniques for nanoparticle separation

Nanoparticle separation techniques have been employed for industrial and research applications for a long time, and several gold-standard techniques have been widely implemented for synthetic nanoparticle and biomolecule separation. These conventional nanoparticle separation techniques can be classified into three main categories: separation using an external field, sieving, and colloidal stability.

External field

Nanoparticles have intrinsic properties, such as size, density, magnetic properties, electric properties, and aggregation tendency. These properties could be used to fractionate nanoparticles using external fields, such as centrifugal force or an electric field. These two external forces have been commonly applied for nanoparticle sorting, namely, ultracentrifugation and gel electrophoresis. Ultracentrifugation is the most common technique for separating and purifying nanoparticles. This technique relies on the particle deposition through centrifugal force arising from the rotation of the ultracentrifuge. Ultracentrifugation is able to separate nanoparticles by size and shape, and the resolution can be improved with an additional gradient agent. Sun *et al.* demonstrated the separation of FeCo@C and gold nanocrystals by varying the density gradient and ultracentrifugation duration. Sharma *et al.* were able to separate gold nanoparticles and nanorods based on their shape, as there is a distinction between the hydrodynamic behavior of rods and spherical particles under centrifugation.[27,28] Although this technique is simple, the resolution is limited and requires a density gradient to achieve better separation at the nanoscale. Furthermore, sample loss during purification is inevitable, and exposing the particles to a large gravity force, which can be up to 16 000*g*, increases the tendency for the particles to aggregate.[29] Furthermore, the requirement for specialized equipment for ultracentrifugation makes this technique relatively expensive to apply for nanoparticle separation. Besides ultracentrifugation, gel electrophoresis is also extensively employed for DNA and nanoparticle separation, with high resolution, depending on the gel pore size. Gel electrophoresis separates samples based on their size/charge ratio when the particles are suspended in an electric field. Liu *et al.* demonstrated separation based on the size and shape of silver nanorods and nanoparticles with capillary electrophoresis.[30] Gel electrophoresis has also been shown to separate various metal nanoparticles by size, shape, and charge with high resolution.[31,32] Although it is a gold standard for protein and DNA separation, this technique is batch-limited and requires multiple steps to operate, takes a long time for sample separation, and is cumbersome for sample retrieval.[33]

Sieving

In addition to external fields, physical holes or barriers, such as membranes or columns to filter particles based on their properties, are often used for nanoparticle separation. The commonly used sieving techniques to separate nanoparticles are chromatography and nanofiltration. In chromatography, samples are separated in a mobile phase through a stationary phase, and the rate of separation depends on the partitioning speed of the particle through the stationary phase. There are several types of chromatography for nanoparticle separation, such as size-exclusion, affinity, ion-exchange, and high-performance liquid chromatography.[34] This technique has high separation efficiency, but requires a long time, multiple preparation steps, and specialized beads, antibody and buffers for separations. Wei *et al.* applied size-exclusion chromatography with 100 nm pore polymer-based columns to separate gold nanoparticles with a size range of 5.3 to 38.3 nm.[35] Another sieving technique that relies on a membrane is nanofiltration. This is a simple process for particle separation, which allows particles smaller than certain cut-off sizes to pass through the filter. Different membrane materials have been implemented for nanosized filtration. Benfer *et al.* implemented a filtration technique with a ceramic membrane for nanoparticle separation.[36] A supramolecular membrane has been demonstrated to separate nanoparticles in the sub 5 nm size range, which has the capability to be recycled many times.[37] The filtration technique is fast, requires a small volume of solvent, and can be scaled to large sample separation for industrial application. However, the membranes are prone to clogging, subsequently inducing particle aggregation, which could decrease the throughput of separation. It also requires many steps to separate samples with multiple particle sizes.

Colloidal stability

Another bulk separation method for nanoparticle fractionation is to alter the nanoparticle stability and dispersibility based on size or aggregation tendencies with size-selective precipitation (SSP) or solvent addition. Size-selective precipitation relies on aggregation of nanoparticles caused by the addition of unique solvents tailored to nanoparticle surface chemistry, reactivity, or stability. Most of the nanoparticles are surface-modified to improve stability and dispersion in the solution, commonly by charge or steric hindrance. This stability can be disrupted by introducing non-miscible solvents that result in aggregation. Once the aggregation of the nanoparticle is achieved, centrifugation is performed to isolate the non-aggregated nanoparticles left in the supernatant. Rapid salt-based size precipitation has been applied to separate larger nanocrystals from smaller ones by merely adjusting the concentration of the salt in the sample, without requiring traditional heating or condensation of the mixed solutions.[38] In solvent addition, the dispersibility of nanoparticles is manipulated by adding two solvent systems, a highly miscible solvent and a poorly miscible solvent, which induce aggregation and precipitation of the well-dispersed nanoparticles in a solution. Saunders *et al.* tuned the solubility and dispersibility of nanoparticles through carbon dioxide gas-expanded liquids with non-polar aliphatic ligand hydrocarbons, such as hexane, to aggregate and precipitate gold and silver nanoparticles.[39] In another study, Duggan and Roberts utilized a DMSO solvent system to alter the dispersibility of gold nanoparticles.[40]

Nanoparticle separation in microfluidics

Advantages of microfluidics for nanoparticle separation

Conventional techniques to separate nanoparticles have several limitations that reduce the overall performance of the separation. The traditional ways of nanoparticle sorting, such as chromatography and electrophoresis, require hours of time and a large volume of sample for separation. Some methods, such as selective precipitation and ultracentrifugation, have inevitable sample loss during the separation process, while several sieving sorting techniques, such as SSP, chromatography, and nanofiltration, induce sample aggregation. Microfluidics offers miniaturization of conventional techniques, which reduces the minimum sample volume, as well as introducing improvements in the duration and resolution of separation. Microfluidics provides continuous separation for multiple sample sizes and allows for minimum aggregation and sample loss during the separation process. Microfluidics also offers superiority beyond the separation process, as it is able to give real-time control, such as size control, by modulating the experimental parameters, such as the buffer solution and the external field. Furthermore, microfluidics also provides a low-cost solution for nanoparticle and biomolecule separation, which could be easily integrated with other techniques, such as mixing, counting, detection and analysis. On the other hand, nanofluidics has been an emerging area for nanoparticle study, including nanoparticle separation with very high separation efficiency and resolution; however, fabrication of nanofluidic devices is more expensive and complex, as it needs smaller and more precise fabrication to produce submicron-sized channels. Furthermore, nanofluidics for nanoparticle separation holds challenges associated with a very small throughput, such as in nano-DLD with a gap size of 25 nm, which has a flow rate of 0.1–0.2 nL min^{-1}, as compared to ~1 μL min^{-1} in microfluidics.[41] Therefore, microfluidics holds the upper hand for nanoparticle separation compared to both conventional techniques and nanofluidics.

Nano-regime separation in microfluidics

Microfluidics for microparticle separation has been well-established and widely applied, mainly for cell separation. There is an increasing trend to push the boundaries of microfluidic separation towards nano-regime separation. However, several microfluidic separation techniques that have been

successfully employed for microparticle separation are facing difficulties with implementation for nanoparticle separation. The commonly known parameters that influence the breakdown of separation in the nano-regime are size, diffusion, conformational structure, surface forces, pH, and buffers. To sort particles, additional forces need to act on the particle to displace it away from its initial position. For sorting forces, such as dielectrophoresis, acoustophoresis, and inertial microfluidics, the effect of size reduction toward the nano-regime exponentially reduces the sorting forces acting on a particle, as the magnitude of the force acting on the particle is largely dependent on size.[42–44] This can be solved by increasing the magnitude and frequency of acoustophoresis and dielectrophoresis to cater for nanoparticle separation.[45,46] The details of the effect of this smaller radius on separation are discussed in the following section for each microfluidic technique. In addition, a smaller size would result in faster Brownian motion of the nanoparticle, which could impede its separation in certain microfluidic techniques.[47] This is especially so when the effect of Brownian motion is more prominent as compared to sorting forces, which results in poor separation resolution. This can be tackled by increasing the primary sorting force or using different approaches to decrease the time-dependent diffusive effects, such as reducing the transit time of the particles within the device. There is a large branch of microfluidics that utilizes the microstructural fabrication of channels, pores, pillar obstacles, and filtration membranes to selectively separate particles by size with sieving or laminar flow-based methods.[48–50] The need to fabricate and characterize these structures at the nanoscale for nanoparticle separation may require specialized and expensive methods, such as e-beam lithography, nanoimprint lithography, or the use of controlled material deposition and growth in pores.[49] Furthermore, unlike microparticles, such as cells, that mostly have relatively round and uniform shapes, nano-biomolecules, such as DNA, RNA, and protein, have unique shapes, structures, topology, and conformations, which increase the difficulties in the sorting process. On top of these challenges, the reduction in size for nanoparticles introduces significant properties and influences that are generally negligible in microparticle separation. Nanoparticles have higher surface to volume ratios, which results in higher surface energy, and hence they become more prone to aggregation as compared to microparticles.[51] This leads to the importance of microfluidic surface treatments, as well as the choice of buffer solutions, to prevent nanoparticle aggregation during separation. Moreover, due to its small size, the electric double layer length of a nanoparticle may be comparable to its size. For example, in deionized water, the Debye length of the nanoparticle is 311 nm, which might be much larger than the size of proteins, DNA, and RNA.[52] This infers that nanoparticle surface interaction forces, which comprise electrostatics,[53] hydrophobic,[54,55] and Van der Waals forces, need to be carefully balanced and understood. As these effects become more prominent, the separation behavior of nanoparticles depends largely on the properties of the surrounding environment, such as materials, solvent, pH, and temperature.[56] These nano-regime properties can be used either to achieve nanoparticle separation or degrade the separation. For instance, separation resolution in most microfluidic techniques can be disrupted by diffusion, while for other techniques, diffusion can be employed as the driving force for nanoparticle separation.[57] Furthermore, the new separation technique of electrostatic sieving can be employed for nanoparticle separation in microfluidics due to the large influence of surface interaction forces on nano-regime microfluidics.[53]

Microfluidic techniques for nanoparticle separation

Microfluidics is able to separate nanoparticles continuously with relatively simple preparation steps compared to traditional methods. These particle-sorting techniques can be classified into active and passive separation.[22] The active technique requires an external field to drive the separation; on the other hand, the passive technique only relies on the inherent properties of microfluidics, such as hydrodynamics, channel geometry, and additionally surface forces for nanoparticle separation. Table 1 below summarizes recent studies on nanoparticle separation using microfluidic techniques.

Active separation

Integration of microfluidics with external fields gives superiority to the separation as it can sort, deflect, or trap the particles based on their intrinsic properties to overcome Brownian motion. Several active separation techniques that have been implemented for nanoparticle separation include field flow fractionation, centrifugal microfluidics, optical techniques, magnetophoresis, acoustophoresis, electrophoresis, dielectrophoresis, ion concentration polarization, and electrohydrodynamic vortices.

Field flow fractionation. Field flow fractionation (FFF) was developed by Giddings *et al.* as a chromatography-like technique with flow injection methods to separate particles based on size by the combination of hydrodynamic forces, Brownian motion, and an external force field.[58] The external force field, which is applied perpendicularly to the direction of the flow, induces the particles to laterally displace to the side walls. At the wall, nanosized particles are mostly affected by Brownian motion, which thereby displaces them away from the wall to an equilibrium position. Eventually, as a result of their parabolic velocity profile, the nanoparticles travel faster than larger particles. There are several external fields commonly used for field flow fractionation, and each method makes use of different intrinsic properties of the nanoparticles, such as magnetic FFF (mFFF), sedimentation FFF (sFFF), flow FFF (F4), thermal FFF (ThFFF), and electrical FFF (eFFF).[25] Although FFF was first developed as a macro-scale technique, miniaturization of FFF is generally able to improve the performance of the separation, particularly in

Table 1 Summary of microfluidic techniques that have been implemented for nanoparticles

Techniques	Mechanism	Separation marker	Nanoparticles separated	Efficiency	Throughput	Advantages	Drawbacks	Ref.
Field flow fractionation	Asymmetrical flow FFF	Size	5–250 nm	87–88%	400–1100 μL min^{-1}	Very high throughput with high separation efficiency	Requires specific sample, solvent or membrane	63 and 64
Centrifugal	Centrifugal force	Size, density	50 nm, 100 nm, and 200 nm	—	500 μm s^{-1} (~7.5 μL min^{-1})	High throughput, does not require density gradient and dilution	Needs centrifugation equipment, not continuous separation	75
Optical	Optical force	Size, refractive index, polarizability	70 nm, 500 nm, and 1 μm	—	100 μm s^{-1} (~0.375 μL min^{-1})	High separation efficiency	Heating and photo damage to particles, low throughput	80
Affinity capture	Surface interaction	Antigenic site, hydrophobicity, charge	100 nm	—	10 μL min^{-1}	High capture efficiency and purity	Expensive antibody, multiple preparation steps	107
Electrophoresis	Uniform electric field	Size, charge	<50 nm	97%	0.4 μL min^{-1}	Very high separation efficiency and resolution	Flow rates change with chemistry (buffer types, wall effects)	116 and 161
Dielectrophoresis	Non-uniform electric field	Polarizability and size	30 nm, 60 nm	85–100%	10 μm s^{-1} (~0.009 μL min^{-1})	High throughput and separation efficiency	Requires high voltage, depends on medium conductivity, very low throughput	124
Magnetophoresis	Magnetic field	Size, magnetic properties	5 nm, 7 nm and 200 nm	90%	300 μL min^{-1}	Very high throughput, requires relatively low cost	Requires long time for magnetic bead antibody labelling	85 and 88
Acoustophoresis	Ultrasonic sound wave	Size, density, compressibility	<200 nm	>90%	1.5–2.8 mm s^{-1} (0.43–0.81 μL min^{-1})	High separation efficiency, controlled cut off separation	Complex fabrication, limited device material to transmit acoustic power efficiently	45
Ion concentration polarization	Electric field	Size, electrophoretic mobility	500 nm, 100 nm	—	0.5 μL min^{-1}	Requires low voltage, does not require internal electrode	Low resolution on small size particles and low throughput	137
Electrohydrodynamic vortices	Travelling waves, ohmic heating	Size, charge	200 nm	~100%	0.033 μL min^{-1}	High separation efficiency	Complex fabrication of microelectrode, low throughput	140
Deterministic lateral displacement	Laminar flow stream	Size, deformability and shape	190 nm, 2 μm and 600 nm	~100% (20 nm resolution)	400 μm s^{-1} (~0.01 μL min^{-1})	Controllable cut off size and simple and efficient technique with very high separation efficiency	Very low throughput, requires precise fabrication, pillar clogging issue	152 and 156
Hydrodynamic filtration	Hydrodynamic sieving	Size	100 nm and 1 μm	—	1 μL min^{-1}	Simple technique, high separation efficiency, medium throughput	Prone to membrane clogging	48
Spiral microfluidics	Dean vortices	Size, shape	590 nm,1.9 μm and 7.32 μm	95%	10 μL min^{-1}	Very high separation efficiency, throughput, and simple technique	Prone to particle–particle interaction and diffusion disruption	162

Table 1 *(continued)*

Techniques	Mechanism	Separation marker	Nanoparticles separated	Efficiency	Throughput	Advantages	Drawbacks	Ref.
Straight inertial microfluidics	Shear and wall lift	Size, shape	590 nm, 780 nm, and 1.9 μm	—	—	Very high throughput, separation efficiency, and simple technique	Prone to particle–particle interaction and diffusion disruption	144
Electrostatic sieving	Electric double layer force	Size, charge	19 nm and 39 nm, 50 nm	97%	0.6 μL min^{-1}	Very high separation efficiency and controllable cut-off size with buffer	Only able to separate nanoparticles in low ionic conditions, low throughput	53 and 163
Bacteria chemotaxis	Chemotaxis diffusion and bacterial motility	Selective adhesion on bacteria	320 nm and 390 nm	81%	2.4×10^5 particles per min (~0.013 μL min^{-1})	Simple and low cost technique	Requires antibody conjugation for selective adhesion to bacteria, very low throughput and relatively medium separation efficiency	164

μ-eFFF.[59–61] Several studies also suggest that there is a shorter analysis time and less peak spreading in miniaturized FFF. Another improvement in FFF towards continuous separation is the development of SPLITT (split flow thin-cell fractionation), which is a modification of the FFF design, achieved by adding a splitter on the inlet and outlet for directing different particles to different outlets, as shown in Fig. 1.[62] The SPLITT technique has been implemented by De Momi *et al.* for environmental fluid separation, which fractionates nanoparticles with sizes from <10 nm to 250 nm from microparticles.[63,64] For the purpose of nanoparticle separation, asymmetric flow FFF, with one crossflow filtration membrane on the bottom surface, draws greater interest as it has been demonstrated to separate nanoparticles efficiently, such as for the characterization of gold,[65,66] silver,[67,68] and non-metallic nanoparticles.[69,70] Field flow fractionation has a very high throughput and high separation efficiency, and has been proven to separate particles ranging from several nanometers to 100 μm in size. However, extensive optimization is required as each field flow fractionation method needs specific external field magnitudes, sample types, solvents, or membranes for performing efficient separation.[71]

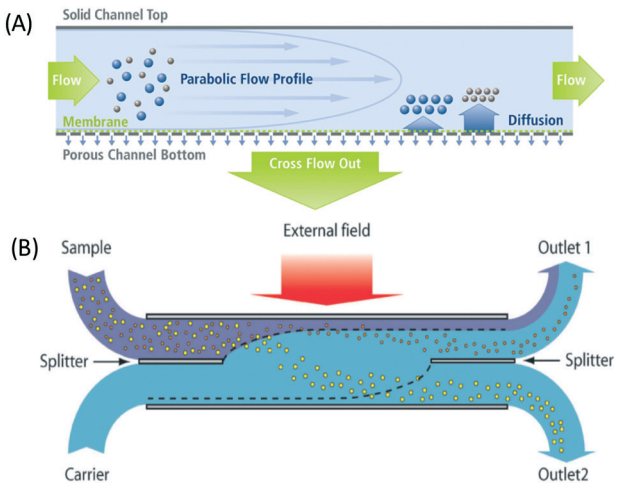

Fig. 1 The field flow fractionation principle combines the parabolic profile, an external field, and diffusion to separate nanoparticles. (A) Asymmetrical flow FFF has a porous semipermeable membrane at the bottom of the channels. Reproduced from ref. 70 (B) Continuous separation using SPLITT, which is a modified FFF achieved by adding a splitter on both inlet and outlet channels. This allows fractionation of particles to different outlet locations based on particle size. Reproduced from ref. 25 with permission from The Royal Society of Chemistry.

Centrifugal microfluidics. In conventional centrifugation, a density gradient often needs to be added to overcome the Rayleigh–Taylor hydrodynamic instability due to colloidal dispersion.[72,73] However, it is difficult to choose a suitable gradient chemical and it requires a longer preparation time to apply the gradient.[74] Arosio *et al.* developed a density-free centrifugal microfluidic technique that does not rely on wall interactions like sedimentation field flow fractionation, and requires a shorter time than conventional centrifugation to sort nanoparticles without the need for sample dilution. In addition to the centrifugal force and hydrodynamic drag force, a buoyancy force is also present on the nanoparticles. The resultant of these forces creates a steady-state lateral velocity (u) that depends on the particle diameter (D_p), particle, fluid density (ρ_p, ρ_f), and distance from the center of rotation (r_d)

$$u = \frac{\rho_p - \rho_f}{18\mu} D_p^{\,2} r_d \omega^2$$

The downstream velocity (v) depends on the hydrodynamic resistance of the channel (R_{tot}), the input and output channel distances, and the area of the channel (A)

$$v = \frac{1}{2}\rho_f \omega^2 \left(r_2^2 - r_1^2\right)\frac{1}{R_{tot}}A$$

Using this method, nanoparticles with sizes of 50 nm, 100 nm, and 200 nm can be separated by a microfluidic flow under a centrifugal force field without applying a density gradient, as the larger or denser particles are deflected towards the outer wall, while the smaller or less dense particles stay near the inner wall, as shown in Fig. 2.[75] Another centrifugal microfluidic technique designed by Kwon *et al.* was able to separate nanoparticles based on the difference in the velocity and duration of centrifugation between 300 nm and 700 nm particles using 2 × 2 inlets and outlets.[74,76] However, the requirement of for centrifugation equipment makes centrifugal microfluidics relatively expensive to apply for nanoparticle separation and it cannot perform continuous separation like other microfluidic techniques.

Optical. Optical manipulation was first developed by Ashkin using optical tweezers to trap and transport individual cells, particles, or molecules by inducing an optical force on the particles based on their size, shape, and refractive index.[77] Currently, the optical force has been widely implemented for particle separation in microfluidics as the application of an optical force perpendicular to the flow is able to deflect the particle trajectories in a microchannel. In the optofluidic system, there are three prominent forces: the drag force that opposes the hydrodynamic flow, the optical scattering force that acts on the particle towards the light propagation direction, and the optical gradient force, which pulls the particle into the peak of the electric fields.[78,79] For a Rayleigh particle,

$$F_{grad}(r) = 2\pi n_2^2 \varepsilon a^3 \left(\frac{m^2-1}{m^2+1}\right)\nabla\left|E^2(r)\right|$$

$$F_{scat}(r) = \frac{n_2}{c}\frac{128\pi^5 a^6}{3\lambda^4}\left(\frac{m^2-1}{m^2+1}\right)^2 I(r)$$

where c is the speed of light, m is the ratio between the refractive index of the particle and the medium, and r is the vector of position. As can be inferred from these equations, nanosized particles have very small scattering forces, as these are related to the power of six of the radius, which means that larger particles can be influenced by both Stokes drag and optical force, while smaller particles are only affected by hydrodynamic forces. Yang *et al.* reported that a combination of hydrodynamic focusing and subsequently optical force treatment could separate a 70 nm particle from 500 nm and 1 μm particles, as illustrated in Fig. 3.[80] They used a single-mode optical fiber with a numerical aperture of 0.12 perpendicular to the hydrodynamic flow direction. This can be achieved as the optical gradient force is strong on particles with a mid-size of 500 nm, and propels the particles to travel to the light source, while particles larger than that (1 μm) are more influenced by the radiation force that forces the particles to move further away from the fiber source. Near the wall, the wall lift force equilibrates the particle position and causes it to move in a straight line after separation. In another study by Shi *et al.*, the separation of 200 nm from 500 nm particles with an interference pattern from double-axicon optofluidics was demonstrated.[81] Separation with an optical force results in high separation efficiency and throughput, although the usage of an optical force, such as optical tweezers, could induce heating or photodamage in the sample.[82]

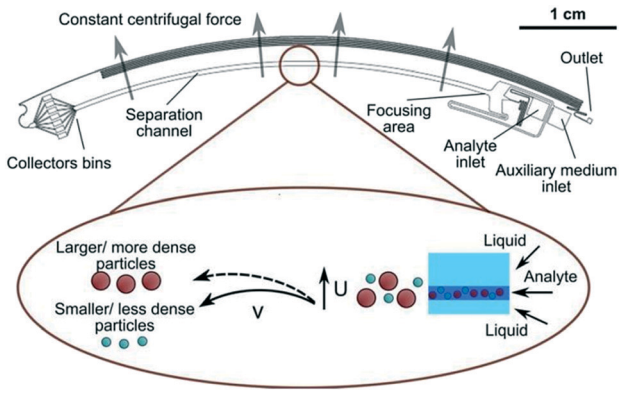

Fig. 2 Density-free centrifugal microfluidic design shows multi-sized nanoparticles at the inlet channel and separation of the particles by the centrifugal force to different collector bins based on size and density. The smaller or less dense particles are less affected by the centrifugal force and stay at the inner wall of the channel, while larger or denser particles are displaced to the outer wall of the channel. Reprinted with permission from ref. 75 Copyright 2014 American Chemical Society.

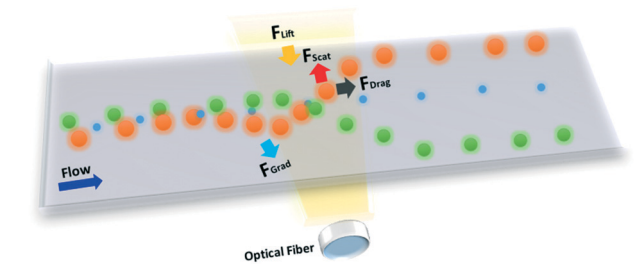

Fig. 3 Focused polydispersed particles from a center flow are fractionated in the microchannel by the optical force perpendicular to the flow. The largest particles (1 μm, orange) are more influenced by the optical scattering force that pushes them away from the fiber source. Particles larger than 200 nm (green) are predominantly influenced by the optical gradient force that manipulates their trajectories towards the optical fiber source, while the smallest particles (50 nm, blue) are unaffected by the optical forces and continue to follow the streamline.

Magnetophoresis

Magnetophoresis utilizes the magnetic susceptibility properties of both particles and fluid for separation. There are two types of magnetophoresis microfluidics based on the source of the magnetic field, one with embedded electromagnetic strips that need to be integrated during fabrication, and another that simply uses an external magnet to actuate magnetic particles. The particle movement under a magnetic field can be classified into positive and negative magnetophoresis. In positive magnetophoresis, particles move towards the higher magnetic field, while in negative magnetophoresis, particles travel away from the magnetic source due to the mismatch between the magnetic susceptibility of the particle and fluids.[83]

The force on a particle in a magnetic field depends on the difference in the magnetic susceptibility of the particle and the fluid ($\Delta\chi = \chi_p - \chi_f$), the magnetic flux density (B), and its gradient (∇B), which is expressed as,[83,84]

$$F_M = \frac{\Delta\chi V_p}{\mu_0}(B\cdot\nabla)B$$

where μ_0 is the vacuum permeability. Munir *et al.* developed a simple tangential PDMS microfluidic channel to separate nanoparticles of size 200 nm, which consisted of 80% magnetite (Fe_2O_3) embedded in a polysaccharide matrix. This microfluidic technique is simple to fabricate as it uses an external magnet as the source of the magnetic field.[85] While paramagnetic particles can be separated easily with a magnetic field, diamagnetic particles can be sorted only after prior conjugation with paramagnetic nanoparticle beads. This system uses antibody-conjugated magnetic beads to specifically bind with target particles, which confers magnetic properties on the samples and allows for their separation when exposed to an external magnetic field.[86,87] Using bead-based magnetophoresis, Lee *et al.* purified hemoglobin with a size of 5 nm from bovine serum albumin *via* a superparamagnetic nanocrystal, as the nanocrystal binds preferentially to hemoglobin through electrostatic interactions, as illustrated in Fig. 4.[88] In another study, an antibody-conjugated superparamagnetic nanoparticle was used to capture the HIV-1 virus, as well as purify protein by mixing it in a microfluidic channel and subsequently separating using magnetic fields.[89,90] This technique does not require large sample elution and can isolate the captured nanoparticles at a high throughput, even though it requires a long time and additional processing for antibody labeling of magnetic beads.

Acoustophoresis. An acoustic force is able to deflect particles depending on their size, density, and compressibility. This acoustic force originates from standing acoustic waves that are generated from a pressure wave of equal magnitude and frequency traveling in the opposite direction, which results in the formation of a node and an antinode. There are two types of acoustic standing waves, bulk and surface acoustic waves (SAWs). Bulk acoustic waves use an ultrasound wavelength that matches the dimension of the microchannel, and this technique has been established for particle separation. However, the material selection for the microchannel is limited due to the requirement for acoustic reflection properties. Meanwhile, surface acoustic waves draw greater interest for nanoparticle separation as they do not require acoustic reflection properties in the material, as they use an interdigitated transducer (IDT), in which the acoustic field, as well as the quantity and location of the pressure node and antinode, can be controlled by the design and location of the IDT.[91–95] SAWs can be further classified into traveling surface acoustic waves (TSAWs) and standing surface acoustic waves (SSAWs).[96] A TSAW is formed from the AC signal that is passed through the interdigitated transducer on piezoelectric substrates, which creates longitudinal leakage waves and generates pressure fluctuation and an acoustic radial force, while a SSAW is formed from the interference of two TSAWs in the opposite direction.[97–100] In a SSAW, the acoustic force on a spherical particle depends on the acoustic pressure p, and the compressibility of the medium β_m as in the following expression,[45]

$$F_a = \frac{\pi^2 p^2 d^3}{12\lambda}\beta_m \phi \sin\left(\frac{4\pi}{\lambda}y\right)$$

where the acoustic pressure can be determined by $p = (PZ/A)^{0.5}$, in which Z is the acoustic impedance, A is the area of the IDT, and P is the power of the input. The ϕ is the acoustic contrast factor, which determines the direction of the particle movement. This factor is expressed as[42]

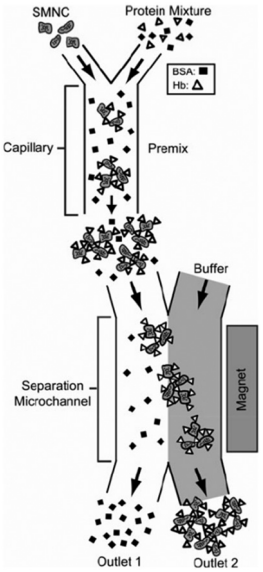

Fig. 4 Superparamagnetic magnetite nanocrystal clusters (SMNC) selectively attach to the hemoglobin, and the conjugated hemoglobin particles are separated from the mixture of unbound bovine serum albumin when the magnetic field is introduced to the channels. Reproduced from ref. 88 with permission from SpringerLink.

$$\phi = \frac{5\rho_p - 2\rho_f}{2\rho_p + \rho_f} - \frac{\beta_p}{\beta_f}$$

Particles with a positive ϕ move towards the node, while particles with a negative ϕ value travel towards the antinode. Using this principle, Collins *et al.* separated nanoparticles with sizes of 500 nm and 300 nm using virtual deterministic lateral displacement by SSAW with high efficiency and throughput.[101] Lee *et al.* reported the separation of 190 nm and 1 μm particles using a standing surface acoustic force with a cut-off particle size separation determined *in situ* by modulating acoustic power and flow speed.[45] Destgeer *et al.* demonstrated TSAW with a frequency of 200 MHz to separate 710 nm from 3 μm particles.[99] While SSAW has a trade-off between particle displacement and the width of the sorting region, TSAW requires a higher strength of acoustic waves and frequency than SSAW to see the effect of separation due to the exponential decrease in acoustic strength.[102] Acoustic separation has high versatility, quick actuation, and is contact-free, biocompatible and has a high separation efficiency; however, application of a high acoustic frequency leads to a high acoustic streaming velocity that can cause the disruption of laminar fluid flow and hence separation in microfluidics.[103]

Affinity-based sorting

Affinity separation has been widely employed to separate particles based on their affinity to specific surfaces, materials, and binding targets, which enables separation of bound particles from unbound ones. This technique can be independently implemented to separate nanoparticles by nanoparticle immobilization or can be integrated with other techniques, such as bead-based separation, using active separation methods like magnetophoresis. Conventionally, nanoparticles can be sorted with affinity chromatography by selectively binding a target that has an affinity to the stationary phase, such as the separation of nanoparticles produced from a molecularly imprinted polymer.[104] In microfluidics, this technique is most commonly used to separate biomolecules, such as proteins and exosomes. As biomolecules harbour unique sites for binding to specific antibodies, this can be utilized for their purification from a mixture of molecules. An example here is the purification of exosomes from a biological sample using the CD63 target in ExoChip microfluidics by way of the immunocapture method.[105] In addition to antibody-based binding, aptamers were also recently developed for selective purification of small molecules, peptides, and viruses. For instance, microfluidics with aptamer-conjugated beads has been used to purify adenosine monophosphate from a mixture of molecules.[106] In addition to specific binding, another type of affinity-based sorting uses non-specific surface adsorption, such as hydrophobic and electrostatic interactions, to capture nanoparticles or biomolecules. A hydrophobic immobilization technique has been demonstrated using a pH-responsive coating of p(NIPAAm-co-pAA) on nanoparticles. This coating induces hydrophobic attachment of the nanoparticles onto the channel surface at low pH.[107] Although non-specific surface adsorption is less specific and weaker than antibody or aptamer binding, specific affinity binding is often expensive as it requires a monoclonal antibody for target capture.[108]

Electrophoresis. Separation using electric fields is one of the most popular techniques for particle separation as the equipment is simple, and there are electrokinetic forces that can be controlled, depending on the setup of the device. While the particles undergo viscous drag inside the fluid, the electric field provides three additional forces, namely electrophoresis, electroosmosis, and dielectrophoresis.[109] The electrophoretic effect refers to the movement of charged particles under an electric field. In the presence of a differential voltage, particles move towards the opposite charge, depending on the electrophoretic mobility of the particle. This electrical mobility depends on the zeta potential (ζ_p) and the dynamic viscosity of the fluid, which enables the method to be used for charge-based separation. The electrophoretic force is expressed as:

$$F_{EP} = 6\pi\zeta_p\varepsilon_f aE$$

where a is the radius and E is the electric field. In a microfluidic channel, this principle is employed in capillary electrophoresis (CE), which is similar to traditional electrophoresis but is implemented in micron-sized channels. Capillary electrophoresis has been implemented for the characterization of synthetic nanoparticles, such as gold nanoparticles and biomolecules, especially DNA and proteins.[110,111] Capillary electrophoresis-evaporative light scattering detection (CE-LSD) has been demonstrated to separate gold nanoparticles with different sizes of 3.5, 6.5, and 10.5 nm.[112] Franze *et al.* utilized capillary electrophoresis with inductively coupled plasma mass spectrophotometry (CE-ICP-MS) to separate and analyze gold particles with sizes from 5–50 nm.[113] Another type of electrophoretic separation method in a microchannel is miniaturizing free-flow electrophoresis (μ-FFE). Unlike capillary electrophoresis, which depends only on the migration rate, as the electric field is parallel to the flow, μ-FFE combines both a pressure-driven flow and electrophoresis with a perpendicular electric field direction to achieve continuous separation.[114] μ-FFE has been shown to separate analytes, such as fluorescent molecules, membrane particles, proteins, and enzymes.[115] Using a T-shaped μ-FFE microfluidic device, Jeon *et al.* separated small dyes of PTS4- and BODIPY2- with sizes in the range of 1 nm with different electrophoretic mobilities associated with different charges.[116] In addition, a bi-directional flow from a combination of electrophoretic movements, with opposing viscoelastic fluid flows, is able to generate a force in the transverse direction, depending on the particle size. With this method, Ranchon *et al.* managed to separate nanoparticles with sizes of 100 nm and 300 nm.[117] Although separation using miniaturized

electrophoresis can reduce the time to several minutes, capillary electrophoresis requires trained users and multiple labor-intensive steps.

Dielectrophoresis. Dielectrophoresis (DEP) employs a non-uniform electric field to induce a force that depends on a particle's electric dipole. This non-uniform electric field can be produced from both alternating current and direct current.[118] The magnitude and direction of the force depends on the gradient of electric fields and particle polarity. There are two different directions of the movements in DEP, which classifies it as positive or negative DEP. Positive DEP occurs when the particle's electric permittivity is smaller than that of the fluid, and the particle is moving towards a higher electric field, while negative DEP has an effect on particles whose electric permittivity is lower than that of the fluid, while travelling towards a low electric field region. There are two types of DEP designs: AC DEP, which uses internal electrodes to generate a non-uniform electric field, and DC insulator DEP (DC iDEP), which uses insulator geometry to create a non-uniform electric field with two electrodes in both ends of the channels.[119] DC iDEP is superior as it does not need an additional external pressure flow, requires simpler fabrication, and is bubble-free inside the separation regions.[120] In DC iDEP, there are two modes of DEP separation, which consist of trapping DEP and streaming DEP. Trapping DEP occurs when the DEP force is higher than the electrokinetic flow that allows trapping of the particles, while streaming DEP occurs when the DEP is weaker than the electrokinetic flow.[121,122] The magnitude of the dielectrophoretic force on the particle depends on the electric field strength (E), the permittivity of both particles and fluid (ε) and the Clausius–Mossotti factor Re(f_{CM}), which is expressed as

$$F_{DEP} = -2\pi\varepsilon_f a^3 \mathrm{Re}(f_{CM}) E\cdot\nabla E$$

where the Clausius–Mossotti factor is expressed as,

$$f_{CM} = \frac{\varepsilon_p^* - \varepsilon_f^*}{\varepsilon_p^* + 2\varepsilon_f^*}$$

in which ε_p^* is the complex permittivity of the particle and ε_f^* is the complex permittivity of the fluid, which can be derived from the permittivity value, the conductivity (σ) and the angular frequency (ω) of the electric field

$$\varepsilon^* = \varepsilon - \frac{j\sigma}{\omega}$$

This Re(f_{CM}) value determines whether the particles undergo positive or negative DEP, with a positive Re(f_{CM}) inferring positive DEP and *vice versa*.[44] Both positive and negative DEP has been widely used for separation of nanoparticles and biomolecules.[123] Computational fluid dynamic simulation has demonstrated the possibility of continuous separation of 30 nm from 60 nm gold nanoparticles using dielectrophoresis.[124] Fig. 5 depicts the nanoparticle separation design using insulator dielectrophoresis. This nanoparticle separation is performed by applying streaming DEP with a low electric field to concentrate the nanoparticles in a highly parallel channel and subsequently trap the particles with a higher electric field at a later stage of the low-branching microfluidic channel.[125] In addition to the branched channel, insulator DEP has been studied to separate nanoparticles with insulating pillars in a microfluidic channel that induces a non-uniform electric field across the pillar gaps to concentrate nanoparticles.[126] Another DEP design to separate nanoparticles is an asymmetric S-shaped ridge, which is able to amplify the electric field by up to 9 times the bulk field. This design, which is reported by Viefhues *et al.*, is able to separate 20 nm and 100 nm nanoparticles.[127] As the DEP separation technique is based on the intrinsic properties of the particles, it does not need an immunochemical labeling process. However, dielectrophoretic particle sorting has a low throughput and is highly dependent on a medium conductivity, which makes it difficult to separate nanoparticles with specific solvent molecules.[128,129] In addition, the voltage requirement is very high, mostly several hundred volts to kilovolts, which leads to the formation of electrothermal flow and joule heating, which can interfere with the separation process.[130] This technique is also challenging as there are various parameters to be optimized for controlled nanoparticle separation, including electric field strength, buffer solutions, surface properties, and geometrical design.

Ion concentration polarization. Nanoparticles can be separated with ion concentration polarization (ICP) by the application of a Nafion nanojunction in microfluidics in the presence of an electric field. The ICP technique has been used to concentrate analytes, such as enzyme substrates, antigens, and proteins. Previously, a review on the principles, fabrication, and application of ICP has been presented.[132] As Nafion selectively transports cations under an electric field through its sulfonated nanopore clusters,

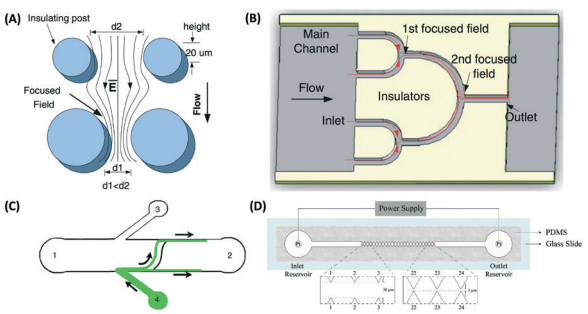

Fig. 5 Designs of DEP for nanoparticle separation. (A) Insulating-pillar DEP and (B) insulating trees for nanoparticle separation. Reproduced from ref. 131 From SpringerOpen (C) DEP nanoparticle separation using ridge structure. Reproduced from ref. 127 with permission from The Royal Society of Chemistry, and (D) sawtooth structures. Reproduced from ref. 46 with permission from The Royal Society of Chemistry

it induces an ion-depletion zone at the anodic sides, with ion enrichment at cathodic sites, as negative ions cannot cross the channel due to the flux of ions caused by diffusion and the electric gradient.[133–135] There are two types of design employed, which are single-channel and dual-channel ICP. Single-channel ICP only uses one channel to create the ion depletion zone, while dual-channel ICP is widely used by connecting two different channels with a Nafion nanojunction.[133] Under an electric field and hydrodynamic pressure in microfluidics, there are several forces acting on the particle, including the hydrodynamic drag, electrophoresis, and dielectrophoresis. In the ion-depleted region, the electric field is amplified significantly, which multiplies the electrophoretic forces acting on the particles.[136] This electrophoretic force deflects the particle from the streamline in proportion to its electrophoretic mobility, as seen in Fig. 6. With this method, Jeon *et al.* were able to demonstrate the separation of 500 nm and 100 nm nanoparticles based on their electrophoretic mobilities, because the electrophoretic effect is amplified 9 times.[137] In addition to nanoparticle separation, the ion depletion zone is also able to remove salts and microparticles from seawater in a branched channel by deflecting the ions away to the neighboring outlet channel for desalination.[138] Although ion concentration polarization only requires a low voltage, as the electric field is amplified in the ion depletion region, the ion depletion region also causes a high ionic concentration gradient that may reduce the nanoparticle separation resolution due to diffusiophoresis.[139]

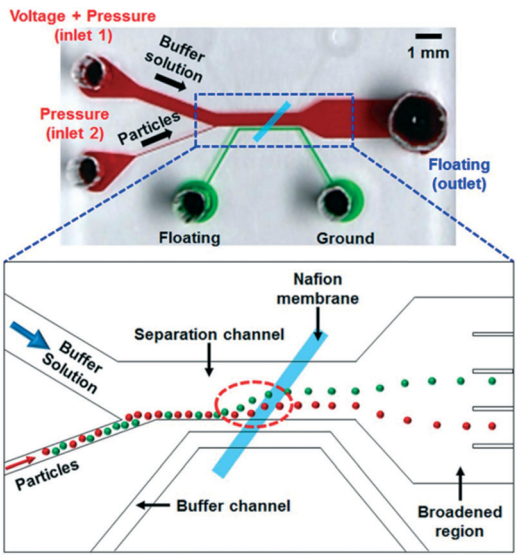

Fig. 6 Nanoparticle separation using ion concentration polarization with a Nafion nanojunction, which generates a repulsion distance, depending on the electric field strength in the ion-depletion region. A low electric field produces a small repulsion distance, while a high electric field traps the nanoparticles in the ion depletion region. Reproduced from ref. 137 with permission from Nature Publishing Group.

Electrohydrodynamic vortices. Microfluidics employs a laminar flow as it has a low Reynolds number due to the small dimensions of the channel. However, an electrohydrodynamic setup with parallel microelectrode strips in microfluidics can disrupt the flow and induce vortices in the channel. Parallel microelectrodes in a transverse direction of the microfluidic channel can generate traveling waves as well as induce ohmic heating, which causes a thermal gradient and eddies in the laminar flow.[140,141] These induced eddies or vortices are then utilized to trap and concentrate nanoparticles, as depicted in Fig. 7. Another form of electrohydrodynamic vortex particle trapping is caused by a combination of hydrodynamic forces and AC electroosmosis on top of the microelectrode strips.[142] In addition to the electroosmosis, the DEP force from the microelectrodes also contributes to the generation of vortices.[143] Boettcher *et al.* trapped 200 nm nanoparticles using this method and provided simulation of the flow. Although the efficiency can be up to 100% trapping, this method needs complex fabrication and has a very low throughput of 2 μL per hour.[140]

Passive separation

Although active techniques have a high separation performance, they are still limited by the need for integration with other equipment to provide an external field, or specific substances, such as antibodies. On the other hand, passive techniques use label-free methods to separate nanoparticles and do not require any external field as the driving force for separation. Instead, hydrodynamic and surface forces are the primary separation mechanism. Six types of passive techniques that have been reported to sort nanoparticles are inertial, spiral, deterministic lateral displacement, hydrodynamic filtration, electrostatic sieving, and bacterial chemotaxis.

Inertial microfluidics. Inertial microfluidics is a passive microfluidic technique that relies on an inertial fluid

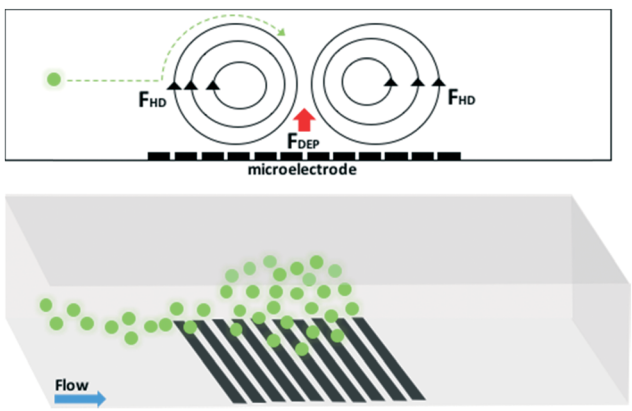

Fig. 7 Nanoparticle trap using electrohydrodynamic vortices formed in a high-frequency electric field generated with parallel microelectrode strips on the channel. The electric field produces travelling waves and ohmic heating, which generates hydrodynamic vortices. Near the microelectrode, the DEP force pushes the particles upward, which supports the particle trapping.

force. There are many types of inertial microfluidics that have been developed, including straight microchannel, spiral microchannel, serpentine microchannel, and expansion contraction array.[43] Inertial microfluidics has been established and widely applied for microparticle separation. However, there are only a few reports on nanosized particle separation. This is due to the challenge of Brownian motion, which can overcome the inertial lift effect. In a straight channel, inertial microfluidics relies on shear inertial lift and wall lift forces that act in opposite directions on the particle. The shear inertial lift force pushes the particle to the wall, while the wall lift counters this force, and the equilibrium of these two forces focuses the particle position in the channel, as illustrated in Fig. 8. The net lift forces (F_L) acting on the particle can be expressed as,

$$F_L = \frac{2\rho v^2 d^4}{D_h^2}$$

in which v is the fluid velocity, ρ is the particle density, D_h is the hydraulic diameter, and d is the particle diameter. From this formula, it can be inferred that the smaller the diameter, the greater the reduction in the inertial lift force. For straight microchannels, the particle velocity focused at the lift equilibrium position can be determined by the particle Reynold number (Re_p), which depends on the Reynold number (Re), and the square of the particle diameter and the channel ratio $\left(\frac{d}{L_C}\right)$

$$Re_p = Re\left(\frac{d}{L_C}\right)^2$$

Different shapes of channel, including circle, square, rectangle, and trapezium have been reported for inertial separation. However, only a high-aspect rectangular channel developed by Bhagat *et al.* has been reported to be able to separate nanoparticles of sizes 590 nm and 780 nm.[144] There is a limit to the minimum nanoparticle size to be separated if only the lift force based on the channel geometry is used. However, by using a viscoelastic fluid medium to generate a medium elastic force, in addition to the wall inertial lift force, nanoparticle separation of sizes 500 nm and 200 nm can be achieved.[145]

Another inertial microfluidic geometry that has been used to separate nanoparticles is spiral channel. This spiral geometry induces centrifugal forces on the particles, causing them to travel outwards. On top of that, in a curved channel with a relatively high Reynold number, a secondary flow is present in the form of two symmetrical vortices that can spread small particles on the channel without affecting larger particles positioned near the outer wall. This force is termed Dean vortices and can be expressed by a Dean number (De),[25]

$$De = Re\sqrt{\frac{H}{2R}}$$

in which R is the radius of the channel curvature and H is the hydraulic diameter of the channels. The velocity of the secondary flow can be expressed as

$$De = 1.8 \times 10^{-4} \times De^{1.63}$$

Five-loop spiral microfluidic channels based on these principles were implemented by Bhagat *et al.*, who demonstrated the sorting of 590 nm from 1.9 μm and 7.32 μm fluorescence-labeled polystyrene beads with a throughput of 10 μL min^{-1}.[147] The inertial microfluidic technique is simple because it only relies on the force from both the fluid and the wall, while also generating a high throughput. However, particle–particle interactions can act as an internal force in disrupting the equilibrium between the fluid and wall lift force, which may lead to a reduction in separation efficiency.[22]

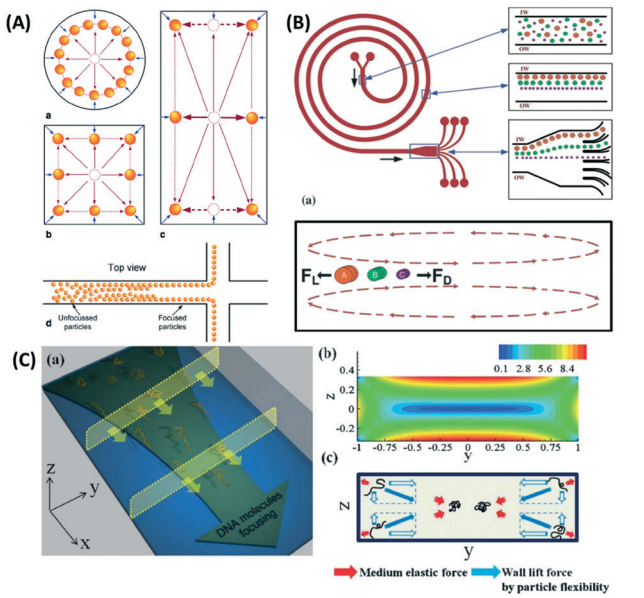

Fig. 8 Inertial force equilibration (A) circular and square channels show uniform particle position near all the side walls, while the rectangular channel inertial force results in a unique particle position only on the left and right side of the walls, which allows it to separate nanoparticles in the branched channel. Reproduced from ref. 144 with permission from SpringerLink (B) Spiral microfluidics separates particles by a combination of the lift force (F_L) and the Dean force (F_D). Larger particles tend to move towards the inner wall, while smaller particles disperse over the channel, as they are influenced more by Dean vortices. Reproduced from ref. 146 with permission from The Royal Society of Chemistry. (C) Inertial microfluidics with viscoelastic fluids concentrates DNA and nanoparticles to the center of the channel through a medium elastic force, in addition to the wall lift force. Reproduced from ref. 145 with permission from The Royal Society of Chemistry.

Deterministic lateral displacement. Deterministic lateral displacement (DLD) consists of a structure of pillar arrays tilted at an angle that generates unique flow streamlines. The DLD technique has been widely used for microparticle separation, such as circulating tumor cells,[148] blood cells,[17] mammalian cells,[149] spores,[18] parasites,[150] and bacteria.[151] Huang *et al.* found that in a laminar flow, the number of streamlines formed in the gap from the row shift could result in size-based separation.[152] Particles larger than the first streamline displace laterally in bumping mode, while particles smaller than the first streamline flow in a zig-zag path through the pillars without lateral displacement, as illustrated in Fig. 9. The cut-off diameter between these trajectories is the critical diameter (D_c) of the device.[153] Davies *et al.* proposed a formula for the critical diameter empirically through experiments with various device gaps (G), shift fractions (ε) and particle diameters.[17]

$$D_c = 1.4G\varepsilon^{0.48}$$

Based on this D_c formula, a device with a small gap or row shift fraction is required to separate nanosized particles. However, a small gap size leads to high channel resistance and difficulty in fabrication, while a low row shift fraction design needs a longer region for separation, which increases the diffusion length. Alternatively, the use of different pillar shapes, such as triangle,[154] I-shaped,[151] or asymmetric gap,[155] could enhance the separation of smaller particles, as the cut-off diameter is smaller than normal circular DLD arrays. A review on deterministic lateral displacement has been previously published.[50] Several attempts to separate submicron particles with DLD have been reported. Huang *et al.*, who first developed DLD, designed a device with a gap of 1.6 μm and a row shift fraction of 0.1 to separate 600 nm and 800 nm polystyrene beads. Santana *et al.* implemented a DLD device with a critical diameter of 250 nm and demonstrated the sorting of 2 μm beads from 190 nm fluorescence-labeled particles[156] Moreover, Zeming *et al.* designed a DLD pillar array with a gap of 2 μm to separate 350 nm particles.[53] Although this technique is simple and has been widely used for microparticles, the presence of a large number of pillars leads to very low throughput and channel clogging issues. Furthermore, for nanosized particles, the effect of diffusion is more prominent, which reduces the separation efficiency by having a large distribution of particles in the outlet channel.[157]

Filtration. Filtration techniques can also be implemented inside a microfluidic channel. Microfluidic filtration techniques require nanosized pores or membranes to separate nanoparticles. There are four classifications of filtration, depending on the structures of the filter, which are hydrodynamic, hydrophoretic, size-exclusion and crossflow filtration.[23] In hydrodynamic filtration, there are multiple branched side channels to pull the particles to different outlets based on their sizes. Hydrophoretic filtration uses ridges on the ceiling and floor of the channel to induce a lateral pressure gradient for particle separation, while size-exclusion filtration uses a series of linear arrays of posts to filter different-sized particles in each tier of the array. The most prominent filtration system is the crossflow filtration, which has its filter array arranged in a direction parallel to the direction of the flow. This gives it the advantage of having reduced clogging issues as compared to other filtration techniques. Davies *et al.* showed separation of 100 nm and 1 μm polystyrene beads with a porous polymer monolith (PPM) membrane with a cut-off size of 500 nm, using pressure-driven flow, as seen in Fig. 10.[48] Chen *et al.* implemented a crossflow filtration silicon microfluidic device with a gap of 800 nm to separate plasma from blood cells,[159] and Amato *et al.* designed reusable microfluidics to separate 3 μm beads from rhodamine 6G with a 3D pillar, with no clogging.[160] A filtration technique with microfluidics is able to filter precise sizes of particles in a small sample volume; however, the presence of a membrane for filtration induces clogging or particle aggregation, which could decrease the throughput of separation and render it non-reusable.

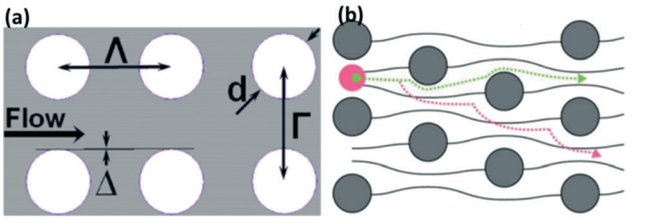

Fig. 9 Nanoparticles can be separated with a deterministic lateral displacement device. (A) Shows DLD design parameters, with d as pillar diameter, and Γ and Λ as row and column periods, respectively, while Δ is the shift fraction. Reproduced with permission from ref. 156 (B) Nanoparticles whose diameter is less than the critical diameter move in a zig-zag mode, while large particles cross the streamlines and displace laterally in bumping mode. Reproduced from ref. 158 with permission from The Royal Society of Chemistry.

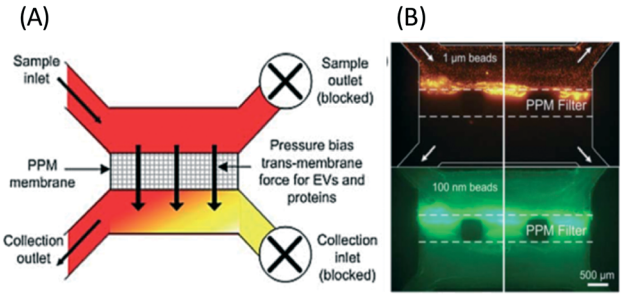

Fig. 10 Microfluidic filtration of nanoparticles can be performed with a PPM filter with pressure-driven separation. (A) The PPM membrane passes particles smaller than the membrane pores to the collection outlet, while larger particles are retained in the sample channel. (B) shows the separation of 100 nm fluorescent beads from 1 μm diameter beads. Reproduced from ref. 48 with permission from The Royal Society of Chemistry.

Electrostatic sieving. Electrostatic sieving employs an electrostatic force arising from the surface potential of nanoparticles and microchannels. Common microfluidic materials, such as silicon and PDMS, have negative surface potentials that attract positive ions in the solution to generate an electric double layer consisting of compact and diffuse layers.[165] As previously discussed, in nanosized particles, the electric double layer length is comparable with the nanoparticle size. This property is important, as the electric double layer (EDL) induces attractive or repulsive electrostatic forces from the wall of the microchannel, which can be employed for nanoparticle separation. This EDL force depends on the Debye length as well as the particle and device's zeta potential, which is expressed as[166]

$$F_{\mathrm{EDL}} = 2\pi\varepsilon\varepsilon_0\kappa\left[\frac{2\psi_{\mathrm{p}}\psi_{\mathrm{s}}\mathrm{e}^{-kD} - \left(\psi_{\mathrm{p}}{}^2 + \psi_{\mathrm{s}}{}^2\right)\mathrm{e}^{-2\kappa D}}{1-\mathrm{e}^{-2\kappa D}}\right]$$

where ψ_{p} is the zeta potential of the particle, while ψ_{s} is the zeta potential of the channel surface, and D is the distance between the particles and the channel; κ is the inverse of the Debye length, which depends on the ionic concentration (c_{i}) and ionic charge (z_{i}), and is expressed by,

$$\kappa = \left[\frac{N_{\mathrm{A}}\mathrm{e}^2}{\varepsilon\varepsilon_0 kT}\sum_{\mathrm{i}} z_{\mathrm{i}}{}^2 c_{\mathrm{i}}{}^{\infty}\right]^{1/2}$$

where N_{A} is the Avogadro number, e is the electron charge, k is the Boltzmann constant and T is the absolute temperature. Nanoparticle trapping and separation using this electrostatic effect have been reported.[167] Regtmeier *et al.* developed a microfluidic technique with overlapping EDL and separated 15 nm and 39 nm carboxylated polystyrene with a 525 nm constriction design by modulating the ionic concentration of the buffer.[163] At low ionic concentrations, the electric double layer length is longer. This results in a higher electrostatic force that allows only smaller particles to pass through the constriction. As the ionic concentration increases, the EDL length is compressed, thereby allowing larger particles to pass through the constriction, as seen in Fig. 11A. In addition to the constriction design, a DLD pillar array with a small gap size shows a similar effect on particle separation. Zeming *et al.* used DLD with a 2 μm gap size to separate nanoparticles up to 50 nm in diameter using deionized water instead of ionic buffers, since this has the lowest ionic strength.[53] The DLD effect alone cannot separate these nanoparticles, as the critical diameter of the DLD is 350 nm according to the formula. This phenomenon is caused by the electrostatic effect arising from the pillar's electric double layer force, which virtually increases the apparent diameter with an EDL distance ($d_{\mathrm{f\text{-}edl}}$) of up to +800 nm in size in deionized water, as illustrated in Fig. 11B.[53] Although this technique is passive and able to modulate separation easily by changing the buffer, it requires the use of low ionic strength buffer to perform nanoparticle separation, since most of the biomolecule samples, such as DNA, proteins, and exosomes, have individual ionic buffers that maintain their structures.

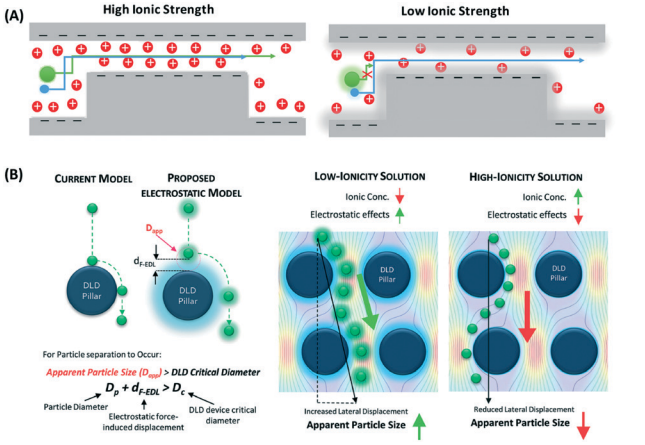

Fig. 11 (A) Nanoparticle separation with electrostatic sieving. In high ionic strength buffer, both large and small particles are able to pass through the constriction. In low ionic strength buffer, large particles cannot pass the ridge due to the strong electrostatic force from the electric double layer, while smaller particles still pass. (B) Microfluidic DLD electrostatic sieving. In DLD, the electrostatic double layer virtually increases the DLD pillar size with $d_{\mathrm{f\text{-}edl}}$ to reduce the critical diameter, resulting in enhanced separation in the presence of low ionic strength buffer solution but not in high ionic strength buffer solution. Reproduced from ref. 53 with permission from The Royal Society of Chemistry.

Cell actuation. Cell actuation can be implemented to drive separation using selective attachment of nanoparticles onto the surfaces of the cells that undergo cell migration induced by a chemoattractant. A review about microfluidics-based chemotaxis for cell migration has been published.[168] The commonly used cell for migration is a bacterial cell as it is actively motile with its cilia or flagella. Suh *et al.* employed cell actuation techniques to separate nanoparticles using the migration of *Escherichia coli* towards the chemoattractant. These migrated bacteria have previously had nanoparticles selectively attached to their surfaces. The compartmentalization of a chemoattractant source and a cell migration pathway is achieved by using three parallel channel designs with polyethylene glycol diacrylate (PEG-DA) porous materials that are able to perform controlled transport of fluids and chemicals from one channel compartment to another, depending on molecular weight.[169] The *E. coli* bacteria is spread in the middle channel with the buffer in the left channel, while the right channel contains the chemoattractant, casamino acid. Selective attachment of nanoparticles is performed *via* biotin-conjugated anti-lipopolysaccharide, which selectively binds the 390 nm streptavidin-coated nanoparticles to *E. coli* bacteria, leaving behind the 320 nm uncoated nanoparticles, as illustrated in Fig. 12. This technique can separate nanoparticles with an efficiency of 81%.[164] Although this autonomous separation using bacteria is simple and does not need any external equipment, it requires a specific binding mechanism between nanoparticles and bacteria, even though the author also

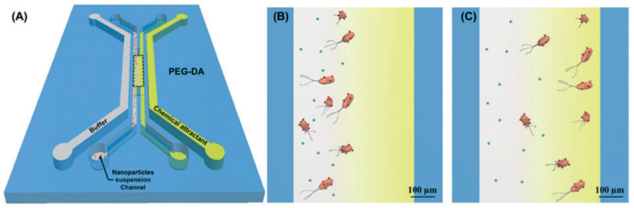

Fig. 12 Microfluidic bacterial chemotaxis for autonomous separation of nanoparticles. (A) Channel designs for modulated diffusion of chemoattractant (B) selective attachment of nanoparticle to *E. coli* bacteria (C) chemotaxis migration of *E. coli* with attached nanoparticles. Reproduced from ref. 164 with permission from The Royal Society of Chemistry.

demonstrated charge-based separation *via* electrostatic interaction on 1000 nm polystyrene beads.

Microfluidic nanoparticle separation applications

As microfluidic technology for nanoparticle separation is superior to conventional techniques, microfluidic techniques draw great interest for several potential applications, ranging from the purification of monodisperse nanoparticles for various industries, and waste water treatment, to nano-biomolecule separation, such as DNA, protein, virus, and exosome isolation.

Biomolecule separation

The ability of microfluidics to separate nanoparticles can also be applied to the separation of biomolecules, such as DNA, proteins, viruses, and exosomes, which has significance in healthcare fields, such as medical diagnostics and therapeutics. These molecules and particles are more complex than synthetic nanoparticles because they can be easily degraded in unsuitable or harsh environments and do not have rigid forms. As it is more difficult to separate such molecules, current approaches to biomolecule separation still largely rely on external fields or immunological techniques, as they have the highest separation efficiency.

DNA. The separation of DNA is important for the detection of disease biomarkers, such as genetic mutations. Furthermore, isolation of DNA is also useful for purification of DNA segments from DNA recombination in research settings. DNA has a size ranging from the nanometer to the micron scale, and can form several complex topologies and secondary structures. A commonly applied technique for DNA separation is gel electrophoresis, which has high reproducibility and efficiency. However, gel electrophoresis is a time-consuming process as it requires ~2 hours, is performed in batch mode, and needs additional sample handling to retrieve the DNA after the separation process. Microfluidics has been developed as a superior alternative to separate DNA. Both active and passive microfluidics have been implemented for a DNA separation platform.[170] The active microfluidic techniques include electrophoresis and dielectrophoresis. Minc *et al.* performed the separation of λ and T4 bacteriophage genomes by electrophoresis in a self-assembled magnetic matrix column microfluidic system with high reproducibility.[171] DNA separation can be achieved using DEP trapping in microfluidic ridges to sort different sizes and topologies, such as linear, plasmid, and mini-circle; a DNA–protein complex has also been reported.[172] Recently, Ranchon *et al.* utilized electric fields and a bidirectional viscoelastic fluid flow to create a modulation of a transverse force to separate DNA with respect to the wall and subsequently enrich by more than 1000× with a funnel in only 15 minutes with high resolution.[117] Passive techniques have also been implemented for DNA separation. Austin *et al.* designed an asymmetric two-dimensional array post and used Brownian motion to separate DNA based on size. Smaller DNA has higher diffusion rates as compared to larger DNA sizes, which results in the lateral displacement of smaller but not larger DNA.[173] Recently, Chen *et al.* were able to apply a label-free passive deterministic lateral displacement technique to continuously concentrate genomic-length DNA by increasing the genome's shear modulus with 10% polyethylene glycol.[174] Kim *et al.* employed a viscoelastic fluid flow to concentrate DNA towards the center of a microfluidic channel by both a flexibility-induced wall lift force and a fluid elastic force.[145]

Protein. Protein separation is also essential for medical diagnostics and disease detection. Various proteins have different sizes and isoelectric points that can be used for the separation process. Traditional techniques to purify proteins include SDS-PAGE and 2D electrophoresis. Other common methods to separate proteins are chromatography and immunological capture using bead-based techniques or protein immobilization. Protein separation using microfluidics has been developed especially because of the need for a low sample volume, and the common microfluidic protein separation is achieved based on the isoelectric points and electric mobility. Wen *et al.* developed free-flow isoelectrics, focusing on a triangular microfluidic device to separate proteins based on their isoelectric point with a 350 V cm^{-1} electric field and a high flow rate.[175] Herzog *et al.* developed an integrated microfluidic system for protein or peptide separation with free-flow isoelectric focusing, labeling, and an isoelectric point sensor.[176] Continuous separation of four types of amino acid and proteins, such as trypsin inhibitor and RNAse A, using microflow electrophoresis (μ-FFE) and its simulation has been reported.[177] In another report, Tekin and Gijs separated and purified proteins using antibody-conjugated magnetic nanoparticles with magnetophoresis.[90] DEP can also be used for protein fractionation, as a simulation and an experiment to concentrate protein using insulator-based DEP has been shown.[178,179] Nakano *et al.* concentrated IgG antibodies with streaming DEP in a pH range of 6–8 on microfluidic pillar arrays, which coincided well with the simulation study.[180]

Virus

A virus is an agent that causes disease, such as HIV, Ebola, Zika, and SARS. Detection of viral particles has important

implications for medical diagnostics. However, isolation of a virus is difficult due to the diversity of virus sizes from small sizes of 20 nm to 400 nm, different shapes, surface charges, genome types, and protein contents.[181] Furthermore, a virus sample is extracted from complex bodily fluids, such as blood, urine, and saliva, and requires purification from large cells or contaminants for accurate disease detection, as reported for HIV and dengue virus detection.[182,183] Although ultrafiltration with a charge-based membrane is effective for viral particle separation, this technique is relatively expensive and needs additional elution steps, while still requiring the use of a suitable charge, buffer, and pH for the different types of viruses.[184] Both passive and active microfluidic separation can be utilized to concentrate the virus and eliminate the contaminant in the samples. Wang *et al.* implemented passive microfluidic size-exclusion filtration to separate HIV virus from blood.[185] Active microfluidic techniques for the enrichment of Sindbis viruses with a size of ~70 nm has been achieved using iDEP in a sawtooth structured gradient.[46] Acoustic microfluidics has also enabled dengue virus separation from cells with an efficiency of 70%.[186]

Exosome. An exosome is an extracellular vesicle with a lipid membrane bilayer, which has an important role in cell communication, as it carries signals and miRNA from one cell to another, especially in cancer developments.[187] Moreover, its presence in extracellular fluid, blood, and urine provides a platform for liquid biopsy for cancer diagnosis.[188] Unlike DNA and protein, exosome separation has not been explored extensively. Exosome separation is challenging, as there are other microvesicles or debris in the size range of exosomes, in addition to its small size ranging from 50 nm to 150 nm.[189,190] Conventionally, ultracentrifugation is used for exosome isolation; however, it is a time-consuming process with a complex protocol and has a low separation efficiency.[191] In microfluidics, there are currently both passive and active methods that have been developed for exosome separation. Three passive microfluidic techniques to separate exosomes, namely immunological separation, sieving and trapping, and DLD, are depicted in Fig. 13. On the other hand, the active technique of acoustophoresis has been reported for exosome separation.[192,193] Although label-free methods can separate small microvesicles based on size, the exosomes must be labeled using an antibody, as there are many types of extracellular vesicles, such as apoptotic and membrane vesicles, whose size overlaps with those of exosomes in the samples.[194] Using an immunological separation method, membrane-bound proteins are used in a microfluidic immunoaffinity system to separate exosomes from blood serum and extracellular cell culture medium.[105,125] This immunological separation can also achieve multiplex exosome detection, which has been implemented for ovarian cancer diagnosis.[195]

With label-free sieving methods, exosome separation with PPM-based membrane filtration from whole blood is demonstrated. The sieving technique can be performed with undiluted samples, such as whole blood, but it has a low recovery and sometimes there is damage to the vesicles.[48] In addition to sieving, Wang *et al.* proposed a microfluidic trapping system with a ciliated micropost in a microfluidic device. The cilia on the pillars capture and immobilize the exosome, while larger structures flow around these microstructures. The immobilization of 83 nm lipid vesicles from 120 nm lipid vesicles and 500 nm nanoparticles was demonstrated.[49] Although this technique can capture high purity exosomes from samples, it requires a long time for the separation, as the sample must be diluted to avoid device clogging. While several passive separations have been reported, there are fewer reports about active techniques for exosome separation. The active separation of exosomes from blood components using acoustic purification has been developed using a pair of interdigitated transducers (IDT), generating symmetric surface acoustic waves with a high ultrasound frequency to generate a cut-off size of 200 nm.[45]

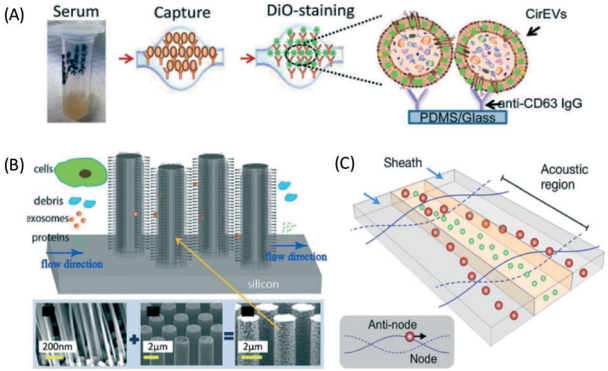

Fig. 13 (A) ExoChip shows anti-CD63 immobilized in a microfluidic surface to capture exosome from serum. Reproduced from ref. 105 with permission from The Royal Society of Chemistry (B) trapping of exosomes with ciliated pillar structure on microfluidic device. Particles larger than cilia pores are not trapped on the cilia while particles much smaller than the pores pass through the structures. The cilia trap particles whose size matches the exosomes and SEM of the ciliated structure on pillar arrays. Reproduced from ref. 49 with permission from The Royal Society of Chemistry. (C) Acoustic forces in microfluidics are able to purify exosomes using a high-frequency field through IDT. Reprinted with permission from ref. 45 Copyright 2015 American Chemical Society.

Monodisperse nanoparticle production

Nanoparticle synthesis is currently shifting towards the modification of individual nanoparticles into higher-ordered structures and nanomaterials for various industrial applications.[9] Metallic nanoparticles, such as gold, silver, and palladium, are utilized as sensors, solar cells, foods, drugs, paints, and other consumer products. Nanoparticle synthesis in these processes often yields polydispersed particles. Therefore, the control of size is crucial for achieving maximum nanoparticle performance, as the physical and chemical properties of these nanoparticles, such as aggregation tendency, depend on their size. For instance, monodispersed nanoparticles have been useful for achieving the maximum catalytic activity of a nanocatalyst in industrial reactions.[196] The cytotoxicity

of gold nanoparticles also depends on their size.[197] Hence, the development of microfluidics to continuously purify monodispersed nanoparticles with high efficiency is beneficial for these industries. This application of microfluidics to purify nanoparticles for industrial purposes has not been implemented as it requires a large volume of sample, and hence high throughput separation is needed for this purpose.

Environmental application

In addition to nanoparticle purification, microfluidic nanoparticle separation has the potential for environmental application, such as wastewater treatment and water desalination. Recently, nanoparticles have started to be used in consumer products, such as foods and cosmetics; therefore, nanoparticles will inevitably be found in domestic wastewater, and the presence of these nanosized particles could be hazardous for both health and environment. In addition to domestic waste, industrial nanoparticle waste must also be treated to avoid exposure of humans or the environment to nanoparticles, as traditional water treatment may not be enough to filter all of this ultra-small nanoparticle waste. For instance, silica nanoparticles are present in electronic chips and integrated circuits, resulting in industrial waste in China and Taiwan.[10] Asymmetric FFF has been reported to separate nanoparticles for environmental applications to fractionate colloids, such as pollutants.[198] Another application of microfluidics for environmental application is seawater desalination, such as that demonstrated by ICP, which is able to remove 99% of the salt from seawater with a low energy and cost.[138]

Microfluidic nanoparticle separation challenges

The implementation of nanoparticle separation using microfluidics is still limited because there are several challenges that need to be addressed before it can be widely developed and used for real-world applications. These challenges include nanoparticle diffusion, limited throughput, and detection.

Diffusion. Brownian motion is the random movements of particles in fluids. In a microfluidic channel, a dimensionless number called a Peclet number shows the influence of diffusion on the particle trajectories, from the ratio of advection to the diffusion rate for particles in moving fluids.[47]

$$\mathrm{Pe} = \frac{v\varepsilon L}{D_\mathrm{f}}$$

where L is the channel length and D_f is the diffusion coefficient of the particle, which depends on its size and shape. The Stokes–Einstein relationship expresses the diffusion coefficient as,

$$D_\mathrm{f} = \frac{kT}{3\pi\mu a}$$

in which k is the Boltzmann constant, T is the absolute temperature, and μ is the dynamic viscosity of the fluid. The particle moves without significant diffusion if Pe $\gg$ 1 because the convection influences the movement of the particle much more than diffusion.[156] While several techniques, such as field flow fractionation, employ Brownian motion to perform separation, the diffusion of nanoparticles mostly reduces the separation efficiency in other microfluidic techniques, especially in passive techniques where there is no external force that strongly opposes the Brownian motion. For a nanosized particle, the radius is of the order of 10^{-9}, hence the Peclet number is higher compared to a micron-sized particle in the same channel. A nanoparticle diffusion effect is observed in electrostatic DLD for 50 nm size separation, inertial microfluidics in the separation of 200 nm, and ICP-induced separation of 100 nm nanoparticles, in which the spread of the particle is wider compared to the micron-sized particles, as seen in Fig. 14.[53,137,145]

Throughput. Microfluidics has been proven to have high efficiency for nanoparticle separation. However, compared to conventional methods, the throughput of microfluidic nanoparticle separation techniques still poses a challenge for industrial applications, as it needs to process high volumes of

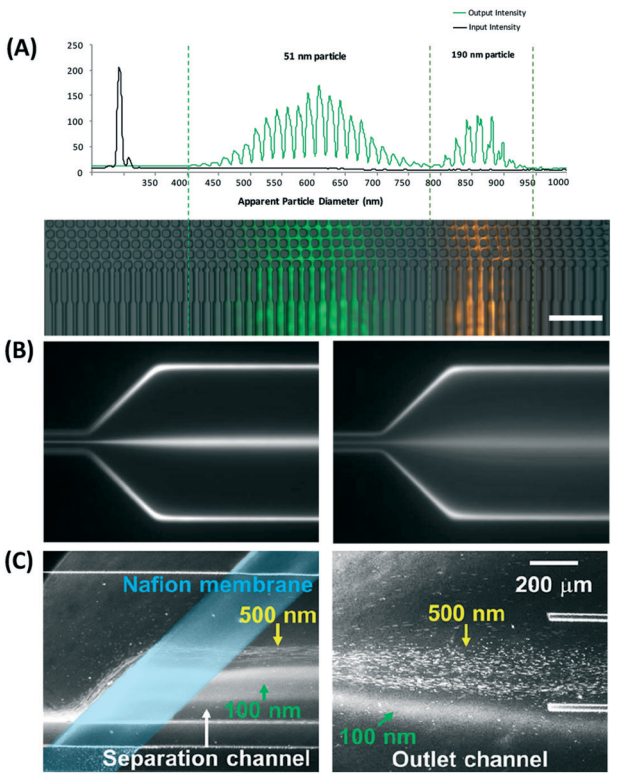

Fig. 14 Wider separation spread caused by Brownian motion of nanoparticles in (A) electrostatic DLD of 50 nm and 190 nm nanoparticle size. Reproduced from ref. 53 with permission from The Royal Society of Chemistry (B) 500 and 200 nm in viscoelastic flow separation. Reproduced from ref. 145 with permission from The Royal Society of Chemistry, and (C) 100 nm nanoparticle size with ion concentration polarization. Reproduced from ref. 137 with permission from Nature Publishing Group.

nanoparticle samples. Microfluidic devices have micron-sized channel dimensions that provide a lower volume of sample to be used for effective separation. The relationship between flow rate and resistance in pressure-driven flow is expressed as,

$$R = \frac{\Delta P}{Q}$$

where R is the fluidic resistance, ΔP is the pressure difference and Q is the flow rate. In a simple rectangular channel, the resistance of a microfluidic device depends on the viscosity (μ), length (L), width (w) and height (h) of the device, and is expressed as[199]

$$R = \frac{12\mu L}{wh^3}\left[1 - \frac{h}{w}\frac{192}{\pi^5}\sum_{n=1,3,5}^{\infty}\frac{1}{n}\tanh\frac{n\pi w}{2h}\right]^{-1}$$

Most microfluidic designs have dimensions of several to a hundred microns for length, width, and height, which results in a high resistance to fluidic movement. For several pressure-driven flow methods, especially passive ones, such as filtration and electrostatic sieving, used for nanoparticle separation, the channel has small pores (down to 2 μm size), which significantly increases their resistance to fluid flow.[155] Other methods that are not driven by pressure differences, such as electrophoresis and electroosmosis, have a slower particle velocity and require high electric fields to increase the throughput. The current approach to increase the throughput is to stack the microfluidic devices in parallel. Inglis *et al.* were able to produce a flow rate of 1 mL min^{-1} by running six DLD devices in parallel for leucocyte enrichment.[200] Khoo *et al.* also stacked three spiral microfluidic devices vertically to develop an ultra-high throughput for the detection and enrichment of circulating tumor cells.[201]

Detection. Compared to micron-sized particle detection, such as cells, nanoparticle detection after separation is more challenging, as it cannot be observed directly under a standard laboratory microscope without staining. There are currently three ways of detecting nanoparticles after separation, and these can be classified into optical, electrochemical, and mass spectrophotometry techniques. These detection techniques can be performed either off-chip or on-chip. While the off-chip method requires collection of the sample after separation in order for it to be analyzed in a detector, the on-chip detection method integrates both separation and detection on the same chip, and is thus more convenient and deemed suitable for lab-on-chip applications.[202] The optical method is the most common method to detect nanoparticles and biomolecules, as they are often tagged by dyes/fluorescence. Several optical methods that have been commonly used for nanoparticle or biomolecule detection are fluorescent imaging, dynamic light scattering (DLS), TEM, and SEM. Within a research setting, commercialized nanoparticles often have fluorescent signals for detection, and a non-fluorescent sample of nanoparticles can first be labeled for observation under a fluorescent microscope. For nanobiomolecule separation, common methods used for detection are dye and immunofluorescence labelling.[105] However, the labeling process for non-fluorescent nanoparticles or biomolecules in real samples, such as detection of exosomes from blood, is difficult as there is only a small number of particles, with much noise, in the sample. Both off-chip and on-chip optical techniques coupled with separation have been reported. Off-chip optical characterization and detection have been performed on nanoparticle samples after their separation with dynamic light scattering and TEM analysis,[203] while on-chip separation-*cum*-detection of DNA and RNA was reported with fluorescent imaging, as well as another study that reported nanoparticle detection with integrated on-chip UV-vis absorption.[204,205] Besides optical methods, biomolecule detection can be achieved through electrochemical detection by sensing the redox activity through a change in current, voltage, and the impedance of the sensors.[206] This technique has been employed for detection of proteins, neurotransmitters, and hormone molecules, and a review on the current development of electrochemical biosensors in microfluidics has been published.[206] On-chip integration of electrochemical sensors and separation in microfluidics has been developed to analyze catecholamine and dopamine-derived DNA adducts using capillary electrophoresis and electrochemical detection.[207,208] Another emerging detection technique for nanoparticles in microfluidics is using mass spectrophotometry, which can identify the molecular weight of the molecules by ionization. Although mass spectrophotometry has high accuracy for molecular identification, the application of this technique for detection in microfluidics is limited by the difficulties in interfacing between microfluidics and mass spectrophotometry. This coupling can be achieved through the integration of emitters on microfluidic devices during fabrication, or using external emitters to couple with electrospray ionization, as reported in previous studies that demonstrate the coupling of external emitters with liquid chromatography and capillary electrophoresis, following separation of a protein sample.[209,210] Furthermore, capillary electrophoresis with inductively coupled plasma mass spectrophotometry (CE-ICP-MS) has been reported to separate and analyze gold particles with sizes from 5–50 nm.[113] A full review on the coupling of mass spectrophotometry and microfluidics has been published.[211,212]

Recently, several innovations on detection techniques were able to achieve nanosized range detection. In optical methods, flow cytometry is one of the popular detection techniques for cells and microparticles as it is fast and accurate; however, conventional flow cytometry has a minimum detection limit of 200–500 nm with a resolution of 100–200 nm, and detection of smaller nanoparticles results in noise overlap from the system. Pospicalova *et al.* developed a dedicated flow cytometry, which is a modified flow cytometry with a different type of light scattering angle, to detect nanoparticles, and successfully performed the detection of fluorescently

labeled exosomes and extracellular vesicles.[213] Additionally, integration of microfluidics with micro-nuclear magnetic resonance (μ-NMR) for on-chip detection after separation has been reported to detect exosomes labeled with magnetic nanoparticles after the separation process.[214] On top of detection with benchtop instruments, portable detection, such as using a smartphone, is recently an emerging field to detect micro/nanoparticles and bioparticles. Wei *et al.* demonstrated the imaging of a single 100 nm nanoparticle and a fluorescently labeled cytomegalovirus using a smartphone with a dongle developed for optical control of light excitation and emission, with embedded image processing for analysis.[215]

Conclusion

Nanoparticle separation plays an important role in many fields, in monodispersed nanoparticle production, water purification, and biomolecule separation. However, conventional methods to separate nanoparticles impose several limitations, such as not being continuous, and requiring multiple steps, a minimum sample volume, a specific buffer, and additional sample handling. Despite still being in the developing stages, both active and passive microfluidic separation techniques are starting to be implemented for nanoparticle and nano-biomolecule separation, as they can overcome these limitations. This brings more opportunities, especially in the medical diagnostic field, for simple, continuous, and faster separation of biomolecules. However, there is a need to explore more possibilities and more prototypes to prove the concept of nanoparticle separation in microfluidics. Microfluidics for nanoparticle separation is more likely to advance towards label-free passive separation, as this is a simpler technique without external fields or surface markers for separation. However, further research is needed to overcome the Brownian motion of nanoparticles in the microchannel to increase the separation efficiency. The application of microfluidics for large industrial nanoparticle separation also still poses a challenge, as improvement in throughput is required to process large sample volumes. Finally, each microfluidic technique has its own advantages and drawbacks for nanoparticle separation, and there is no single technique that can be tailored to all the sample needs.

Acknowledgements

We would like to acknowledge the scholarship from NUS Graduate School for integrative Science and Engineering and funding support from Ministry of Education Academic Research Fund, Singapore (AcRF: R-397-000-183-112).

References

1 B. Sun, E. Marx and N. C. Greenham, *Nano Lett.*, 2003, **3**, 961–963.
2 L. Yuan, X.-H. Lu, X. Xiao, T. Zhai, J. Dai, F. Zhang, B. Hu, X. Wang, L. Gong and J. Chen, *ACS Nano*, 2011, **6**, 656–661.
3 S. Raj, S. Jose, U. Sumod and M. Sabitha, *J. Pharm. BioAllied Sci.*, 2012, **4**, 186.
4 F. von der Kammer, S. Legros, T. Hofmann, E. H. Larsen and K. Loeschner, *TrAC, Trends Anal. Chem.*, 2011, **30**, 425–436.
5 S. Gelperina, K. Kisich, M. D. Iseman and L. Heifets, *Am. J. Respir. Crit. Care Med.*, 2005, **172**, 1487–1490.
6 K. E. Petersen, E. Manangon, J. L. Hood, S. A. Wickline, D. P. Fernandez, W. P. Johnson and B. K. Gale, *Anal. Bioanal. Chem.*, 2014, **406**, 7855–7866.
7 L. Zhang, F. Gu, J. Chan, A. Wang, R. Langer and O. Farokhzad, *Clin. Pharmacol. Ther.*, 2008, **83**, 761–769.
8 M.-C. Daniel and D. Astruc, *Chem. Rev.*, 2004, **104**, 293–346.
9 B. Kowalczyk, I. Lagzi and B. A. Grzybowski, *Curr. Opin. Colloid Interface Sci.*, 2011, **16**, 135–148.
10 Y. Liu, M. Tourbin, S. Lachaize and P. Guiraud, *Chemosphere*, 2013, **92**, 681–687.
11 G. Bystrzejewska-Piotrowska, J. Golimowski and P. L. Urban, *Waste Manage.*, 2009, **29**, 2587–2595.
12 S. Choi, M. Goryll, L. Y. M. Sin, P. K. Wong and J. Chae, *Microfluid. Nanofluid.*, 2011, **10**, 231–247.
13 D. M. Whiley, S. Bialasiewicz, C. Bletchly, C. E. Faux, B. Harrower, A. R. Gould, S. B. Lambert, G. R. Nimmo, M. D. Nissen and T. P. Sloots, *J. Clin. Virol.*, 2009, **45**, 203–204.
14 A. S. Azmi, B. Bao and F. H. Sarkar, *Cancer Metastasis Rev.*, 2013, **32**, 623–642.
15 P. A. Gonzales, T. Pisitkun, J. D. Hoffert, D. Tchapyjnikov, R. A. Star, R. Kleta, N. S. Wang and M. A. Knepper, *J. Am. Soc. Nephrol.*, 2009, **20**, 363–379.
16 Y. Mori, *KONA Powder Part. J.*, 2015, **32**, 102–114.
17 J. A. Davis, D. W. Inglis, K. J. Morton, D. A. Lawrence, L. R. Huang, S. Y. Chou, J. C. Sturm and R. H. Austin, *Proc. Natl. Acad. Sci. U. S. A.*, 2006, **103**, 14779–14784.
18 D. W. Inglis, N. Herman and G. Vesey, *Biomicrofluidics*, 2010, **4**, 024109.
19 H. W. Hou, A. A. S. Bhagat, A. G. L. Chong, P. Mao, K. S. W. Tan, J. Han and C. T. Lim, *Lab Chip*, 2010, **10**, 2605–2613.
20 H. W. Hou, M. E. Warkiani, B. L. Khoo, Z. R. Li, R. A. Soo, D. S.-W. Tan, W.-T. Lim, J. Han, A. A. S. Bhagat and C. T. Lim, *Sci. Rep.*, 2013, **3**, 1259.
21 Z. Wu, B. Willing, J. Bjerketorp, J. K. Jansson and K. Hjort, *Lab Chip*, 2009, **9**, 1193–1199.
22 A. A. S. Bhagat, H. Bow, H. W. Hou, S. J. Tan, J. Han and C. T. Lim, *Med. Biol. Eng. Comput.*, 2010, **48**, 999–1014.
23 C. W. Shields IV, C. D. Reyes and G. P. López, *Lab Chip*, 2015, **15**, 1230–1249.
24 P. Sajeesh and A. K. Sen, *Microfluid. Nanofluid.*, 2014, **17**, 1–52.
25 A. Lenshof and T. Laurell, *Chem. Soc. Rev.*, 2010, **39**, 1203–1217.
26 C. Duan, W. Wang and Q. Xie, *Biomicrofluidics*, 2013, **7**, 026501.
27 X. Sun, S. M. Tabakman, W. S. Seo, L. Zhang, G. Zhang, S. Sherlock, L. Bai and H. Dai, *Angew. Chem., Int. Ed.*, 2009, **48**, 939–942.

28 V. Sharma, K. Park and M. Srinivasarao, *Proc. Natl. Acad. Sci. U. S. A.*, 2009, **106**, 4981–4985.
29 O. Akbulut, C. R. Mace, R. V. Martinez, A. A. Kumar, Z. Nie, M. R. Patton and G. M. Whitesides, *Nano Lett.*, 2012, **12**, 4060–4064.
30 F.-K. Liu, F.-H. Ko, P.-W. Huang, C.-H. Wu and T.-C. Chu, *J. Chromatogr. A*, 2005, **1062**, 139–145.
31 X. Xu, K. K. Caswell, E. Tucker, S. Kabisatpathy, K. L. Brodhacker and W. A. Scrivens, *J. Chromatogr. A*, 2007, **1167**, 35–41.
32 M. Hanauer, S. Pierrat, I. Zins, A. Lotz and C. Sönnichsen, *Nano Lett.*, 2007, **7**, 2881–2885.
33 H. Zorbas, *Bioanalytics: Methods on Molecular Biotechnology and Modern Biotechnology*, Wiley, New York, 2010.
34 E. Heftmann, *Chromatography: Fundamentals and applications of chromatography and related differential migration methods-Part B: Applications*, Elsevier, 2004.
35 G.-T. Wei and F.-K. Liu, *J. Chromatogr. A*, 1999, **836**, 253–260.
36 S. Benfer, P. Arki and G. Tomandl, *Adv. Eng. Mater.*, 2004, **6**, 495–500.
37 E. Krieg, H. Weissman, E. Shirman, E. Shimoni and B. Rybtchinski, *Nat. Nanotechnol.*, 2011, **6**, 141–146.
38 C.-L. Wang, M. Fang, S.-H. Xu and Y.-P. Cui, *Langmuir*, 2009, **26**, 633–638.
39 S. R. Saunders and C. B. Roberts, *Nanotechnology*, 2009, **20**, 475605.
40 J. N. Duggan and C. B. Roberts, *J. Phys. Chem. C*, 2014, **118**, 14595–14605.
41 B. H. Wunsch, J. T. Smith, S. M. Gifford, C. Wang, M. Brink, R. L. Bruce, R. H. Austin, G. Stolovitzky and Y. Astier, *Nat. Nanotechnol.*, 2016, 134, advance online publication.
42 H. Bruus, *Lab Chip*, 2012, **12**, 1014–1021.
43 J. Zhang, S. Yan, D. Yuan, G. Alici, N.-T. Nguyen, M. E. Warkiani and W. Li, *Lab Chip*, 2016, **16**, 10–34.
44 H. Song, J. M. Rosano, Y. Wang, C. J. Garson, B. Prabhakarpandian, K. Pant, G. J. Klarmann, A. Perantoni, L. M. Alvarez and E. Lai, *Lab Chip*, 2015, **15**, 1320–1328.
45 K. Lee, H. Shao, R. Weissleder and H. Lee, *ACS Nano*, 2015, **9**, 2321–2327.
46 J. Ding, R. M. Lawrence, P. V. Jones, B. G. Hogue and M. A. Hayes, *Analyst*, 2016, **141**, 1997–2008.
47 T. M. Squires and S. R. Quake, *Rev. Mod. Phys.*, 2005, 77, 977.
48 R. T. Davies, J. Kim, S. C. Jang, E.-J. Choi, Y. S. Gho and J. Park, *Lab Chip*, 2012, **12**, 5202–5210.
49 Z. Wang, H.-J. Wu, D. Fine, J. Schmulen, Y. Hu, B. Godin, J. X. Zhang and X. Liu, *Lab Chip*, 2013, **13**, 2879–2882.
50 J. McGrath, M. Jimenez and H. Bridle, *Lab Chip*, 2014, **14**, 4139–4158.
51 W. Zhang, in *Nanomaterial*, Springer, 2014, pp. 19–43.
52 Y. Kazoe, K. Mawatari, Y. Sugii and T. Kitamori, *Anal. Chem.*, 2011, **83**, 8152–8157.
53 K. K. Zeming, N. V. Thakor, Y. Zhang and C.-H. Chen, *Lab Chip*, 2016, **16**, 75–85.
54 A. Sánchez-Iglesias, M. Grzelczak, T. Altantzis, B. Goris, J. Pérez-Juste, S. Bals, G. Van Tendeloo, S. H. Donaldson, B. F. Chmelka, J. N. Israelachvili and L. M. Liz-Marzán, *ACS Nano*, 2012, **6**, 11059–11065.
55 S. H. Donaldson, A. Røyne, K. Kristiansen, M. V. Rapp, S. Das, M. A. Gebbie, D. W. Lee, P. Stock, M. Valtiner and J. Israelachvili, *Langmuir*, 2015, **31**, 2051–2064.
56 M. Napoli, P. Atzberger and S. Pennathur, *Microfluid. Nanofluid.*, 2011, **10**, 69–80.
57 C. Zhao and X. Cheng, *Biomicrofluidics*, 2011, **5**, 032004.
58 J. C. Giddings, *Science*, 1993, **260**, 1456–1465.
59 A. I. Lao, D. Trau and I.-M. Hsing, *Anal. Chem.*, 2002, **74**, 5364–5369.
60 T. Shendruk and G. Slater, *J. Chromatogr. A*, 2012, **1233**, 100–108.
61 H. J. Sant and B. K. Gale, *J. Chromatogr. A*, 2006, **1104**, 282–290.
62 N. Narayanan, A. Saldanha and B. K. Gale, *Lab Chip*, 2006, **6**, 105–114.
63 A. De Momi and J. R. Lead, *Sci. Total Environ.*, 2008, **405**, 317–323.
64 A. De Momi and J. R. Lead, *Environ. Sci. Technol.*, 2006, **40**, 6738–6743.
65 B. Schmidt, K. Loeschner, N. Hadrup, A. Mortensen, J. J. Sloth, C. Bender Koch and E. H. Larsen, *Anal. Chem.*, 2011, **83**, 2461–2468.
66 L. Calzolai, D. Gilliland, C. P. Garcìa and F. Rossi, *J. Chromatogr. A*, 2011, **1218**, 4234–4239.
67 H. Hagendorfer, R. Kaegi, M. Parlinska, B. Sinnet, C. Ludwig and A. Ulrich, *Anal. Chem.*, 2012, **84**, 2678–2685.
68 K. Loeschner, J. Navratilova, S. Legros, S. Wagner, R. Grombe, J. Snell, F. von der Kammer and E. H. Larsen, *J. Chromatogr. A*, 2013, **1272**, 116–125.
69 J. Heroult, V. Nischwitz, D. Bartczak and H. Goenaga-Infante, *Anal. Bioanal. Chem.*, 2014, **406**, 3919–3927.
70 D. Müller, S. Cattaneo, F. Meier, R. Welz and A. J. de Mello, *Front. Chem.*, 2015, **3**, 45.
71 F. A. Messaud, R. D. Sanderson, J. R. Runyon, T. Otte, H. Pasch and S. K. R. Williams, *Prog. Polym. Sci.*, 2009, **34**, 351–368.
72 A. Wysocki, C. P. Royall, R. G. Winkler, G. Gompper, H. Tanaka, A. van Blaaderen and H. Lowen, *Soft Matter*, 2009, **5**, 1340–1344.
73 D. H. Sharp, *Phys. D*, 1984, **12**, 3–18.
74 B. H. Kwon, H. H. Kim, J. H. Park, D. H. Yoon, M. C. Kim, S. Sheard, K. Morten and J. S. Go, *Jpn. J. Appl. Phys.*, 2013, **52**, 026601.
75 P. Arosio, T. Müller, L. Mahadevan and T. P. Knowles, *Nano Lett.*, 2014, **14**, 2365–2371.
76 J. B. Ha, Y. K. Bahk, S. H. Yoon, J. H. Lee, E. H. Jeong, S. Y. Yoon, T. Arakawa, J. S. Ko, B. S. Shin, K. C. Kim, J. S. Boo, S. Shoji and J. S. Go, *International Solid-State Sensors, Actuators and Microsystems Conference*, 2007, pp. 927–930, DOI: 10.1109/SENSOR.2007.4300283.
77 A. Ashkin, *Phys. Rev. Lett.*, 1970, **24**, 156.
78 K. S. Lee, J. H. Jung, B. H. Ha, H. J. Sung and S. S. Kim, *Appl. Phys. Lett.*, 2014, **105**, 071908.

79 K. S. Lee, S. Y. Yoon, K. H. Lee, S. B. Kim, H. J. Sung and S. S. Kim, *J. Opt. Soc. Am. B*, 2012, **29**, 407–414.
80 Y. Yang, Y. Shi, L. Chin, J. Zhang, D. Tsai and A. Liu, *The 17th International Conference on Transducers & Eurosensors XXVII*, 2013, pp. 2122–2125.
81 Y. Shi, S. Xiong, L. Chin, M. Ren and A. Liu, *IEEE 27th International Conference on Micro Electro Mechanical Systems (MEMS)*, 2014, pp. 1015–1018.
82 H. Zhang and K.-K. Liu, *J. R. Soc., Interface*, 2008, **5**, 671–690.
83 M. Hejazian and N.-T. Nguyen, *Lab Chip*, 2015, **15**, 2998–3005.
84 M. A. Gijs, F. Lacharme and U. Lehmann, *Chem. Rev.*, 2009, **110**, 1518–1563.
85 A. Munir, Z. Zhu, J. Wang and H. S. Zhou, *IET Nanobiotechnol.*, 2014, **8**, 102–110.
86 A. Munir, J. Wang, Z. Li and H. S. Zhou, *Microfluid. Nanofluid.*, 2010, **8**, 641–652.
87 B. Le Drogoff, L. Clime and T. Veres, *Microfluid. Nanofluid.*, 2008, **5**, 373–381.
88 S. H. S. Lee, T. A. Hatton and S. A. Khan, *Microfluid. Nanofluid.*, 2011, **11**, 429–438.
89 G. D. Chen, C. J. Alberts, W. Rodriguez and M. Toner, *Anal. Chem.*, 2009, **82**, 723–728.
90 H. C. Tekin and M. A. Gijs, *Lab Chip*, 2013, **13**, 4711–4739.
91 L. Ren, Y. Chen, P. Li, Z. Mao, P.-H. Huang, J. Rufo, F. Guo, L. Wang, J. P. McCoy and S. J. Levine, *Lab Chip*, 2015, **15**, 3870–3879.
92 X. Ding, S.-C. S. Lin, M. I. Lapsley, S. Li, X. Guo, C. Y. Chan, I. K. Chiang, L. Wang, J. P. McCoy and T. J. Huang, *Lab Chip*, 2012, **12**, 4228–4231.
93 L. Y. Yeo and J. R. Friend, *Annu. Rev. Fluid Mech.*, 2014, **46**, 379–406.
94 X. Ding, Z. Peng, S.-C. S. Lin, M. Geri, S. Li, P. Li, Y. Chen, M. Dao, S. Suresh and T. J. Huang, *Proc. Natl. Acad. Sci. U. S. A.*, 2014, **111**, 12992–12997.
95 P. Li, Z. Mao, Z. Peng, L. Zhou, Y. Chen, P.-H. Huang, C. I. Truica, J. J. Drabick, W. S. El-Deiry and M. Dao, *Proc. Natl. Acad. Sci. U. S. A.*, 2015, **112**, 4970–4975.
96 X. Ding, P. Li, S.-C. S. Lin, Z. S. Stratton, N. Nama, F. Guo, D. Slotcavage, X. Mao, J. Shi, F. Costanzo and T. J. Huang, *Lab Chip*, 2013, **13**, 3626–3649.
97 G. Destgeer, K. H. Lee, J. H. Jung, A. Alazzam and H. J. Sung, *Lab Chip*, 2013, **13**, 4210–4216.
98 G. Destgeer, B. H. Ha, J. Park, J. H. Jung, A. Alazzam and H. J. Sung, *Phys. Procedia*, 2015, **70**, 34–37.
99 G. Destgeer, B. H. Ha, J. H. Jung and H. J. Sung, *Lab Chip*, 2014, **14**, 4665–4672.
100 J. Shi, H. Huang, Z. Stratton, Y. Huang and T. J. Huang, *Lab Chip*, 2009, **9**, 3354–3359.
101 D. J. Collins, T. Alan and A. Neild, *Lab Chip*, 2014, **14**, 1595–1603.
102 D. J. Collins, A. Neild and Y. Ai, *Lab Chip*, 2016, **16**, 471–479.
103 M. Wiklund, R. Green and M. Ohlin, *Lab Chip*, 2012, **12**, 2438–2451.
104 A. R. Guerreiro, I. Chianella, E. Piletska, M. J. Whitcombe and S. A. Piletsky, *Biosens. Bioelectron.*, 2009, **24**, 2740–2743.
105 S. S. Kanwar, C. J. Dunlay, D. M. Simeone and S. Nagrath, *Lab Chip*, 2014, **14**, 1891–1900.
106 T. H. Nguyen, R. Pei, M. Stojanovic and Q. Lin, *Sens. Actuators, B*, 2011, **155**, 58–66.
107 M. Ebara, J. M. Hoffman, A. S. Hoffman, P. S. Stayton and J. J. Lai, *Langmuir*, 2013, **29**, 5388–5393.
108 X. Huang, Y. Zhu, X. Zhang, Z. Bao, D. Y. Lei, W. Yu, J. Dai and Y. Wang, *Sens. Actuators, B*, 2016, **222**, 106–111.
109 O. D. Velev, S. Gangwal and D. N. Petsev, *Annu. Rep. Prog. Chem., Sect. C: Phys. Chem.*, 2009, **105**, 213–246.
110 L. Trapiella-Alfonso, F. d'Orlyé and A. Varenne, *Anal. Bioanal. Chem.*, 2016, **408**, 2669–2675.
111 F.-K. Liu, Y.-Y. Lin and C.-H. Wu, *Anal. Chim. Acta*, 2005, **528**, 249–254.
112 M. Bouri, R. Salghi, M. Algarra, M. Zougagh and A. Rios, *RSC Adv.*, 2015, **5**, 16672–16677.
113 B. Franze and C. Engelhard, *Anal. Chem.*, 2014, **86**, 5713–5720.
114 R. T. Turgeon and M. T. Bowser, *Anal. Bioanal. Chem.*, 2009, **394**, 187–198.
115 D. Kohlheyer, G. A. J. Besselink, S. Schlautmann and R. B. M. Schasfoort, *Lab Chip*, 2006, **6**, 374–380.
116 H. Jeon, Y. Kim and G. Lim, *Sci. Rep.*, 2016, **6**, 19911.
117 H. Ranchon, R. Malbec, V. Picot, A. Boutonnet, P. Terrapanich, P. Joseph, T. Leichlé and A. Bancaud, *Lab Chip*, 2016, **16**, 1243–1253.
118 B. Çetin and D. Li, *Electrophoresis*, 2011, **32**, 2410–2427.
119 T. Z. Jubery, S. K. Srivastava and P. Dutta, *Electrophoresis*, 2014, **35**, 691–713.
120 S. K. Srivastava, J. L. Baylon-Cardiel, B. H. Lapizco-Encinas and A. R. Minerick, *J. Chromatogr. A*, 2011, **1218**, 1780–1789.
121 E. B. Cummings, *IEEE Eng. Med. Biol. Mag.*, 2003, **22**, 75–84.
122 E. B. Cummings, *IEEE Eng. Med. Biol. Mag.*, 2003, **22**, 75–84.
123 B. H. Lapizco-Encinas and M. Rito-Palomares, *Electrophoresis*, 2007, **28**, 4521–4538.
124 S. Dash, S. Mohanty, S. Pradhan and B. Mishra, *J. Taiwan Inst. Chem. Eng.*, 2015, **58**, 39–48.
125 C. Chen, J. Skog, C.-H. Hsu, R. T. Lessard, L. Balaj, T. Wurdinger, B. S. Carter, X. O. Breakefield, M. Toner and D. Irimia, *Lab Chip*, 2010, **10**, 505–511.
126 S. Dash and S. Mohanty, *Electrophoresis*, 2014, **35**, 2656–2672.
127 M. Viefhues, R. Eichhorn, E. Fredrich, J. Regtmeier and D. Anselmetti, *Lab Chip*, 2012, **12**, 485–494.
128 K. F. Hoettges, M. B. McDonnell and M. P. Hughes, *Electrophoresis*, 2014, **35**, 467–473.
129 B. H. Lapizco-Encinas, B. A. Simmons, E. B. Cummings and Y. Fintschenko, *Anal. Chem.*, 2004, **76**, 1571–1579.
130 B. G. Hawkins and B. J. Kirby, *Electrophoresis*, 2010, **31**, 3622–3633.
131 D. Chen, H. Du and C. Y. Tay, *Nanoscale Res. Lett.*, 2010, **5**, 55–60.
132 S. J. Kim, Y.-A. Song and J. Han, *Chem. Soc. Rev.*, 2010, **39**, 912–922.

133 M. Kim, M. Jia and T. Kim, *Analyst*, 2013, **138**, 1370–1378.
134 S. H. Ko, Y.-A. Song, S. J. Kim, M. Kim, J. Han and K. H. Kang, *Lab Chip*, 2012, **12**, 4472–4482.
135 S. J. Kim, Y.-C. Wang, J. H. Lee, H. Jang and J. Han, *Phys. Rev. Lett.*, 2007, **99**, 044501.
136 S. J. Kim, L. D. Li and J. Han, *Langmuir*, 2009, **25**, 7759–7765.
137 H. Jeon, H. Lee, K. H. Kang and G. Lim, *Sci. Rep.*, 2013, **3**, 3483.
138 S. J. Kim, S. H. Ko, K. H. Kang and J. Han, *Nat. Nanotechnol.*, 2010, **5**, 297–301.
139 R. A. Rica and M. Z. Bazant, *Phys. Fluids*, 2010, **22**, 112109.
140 M. Boettcher, S. Schmidt, A. Latz, M. Jaeger, M. Stuke and C. Duschl, *J. Phys.: Condens. Matter*, 2011, **23**, 324101.
141 M. Felten, W. Staroske, M. S. Jaeger, P. Schwille and C. Duschl, *Electrophoresis*, 2008, **29**, 2987–2996.
142 M. N. Mohtar, K. F. Hoettges and M. P. Hughes, *Electrophoresis*, 2014, **35**, 345–351.
143 N. G. Green and H. Morgan, *J. Phys. D: Appl. Phys.*, 1998, **31**, L25.
144 A. A. S. Bhagat, S. S. Kuntaegowdanahalli and I. Papautsky, *Microfluid. Nanofluid.*, 2009, **7**, 217–226.
145 J. Y. Kim, S. W. Ahn, S. S. Lee and J. M. Kim, *Lab Chip*, 2012, **12**, 2807–2814.
146 S. S. Kuntaegowdanahalli, A. A. S. Bhagat, G. Kumar and I. Papautsky, *Lab Chip*, 2009, **9**, 2973–2980.
147 A. A. S. Bhagat, S. S. Kuntaegowdanahalli and I. Papautsky, *Lab Chip*, 2008, **8**, 1906–1914.
148 Z. Liu, F. Huang, J. Du, W. Shu, H. Feng, X. Xu and Y. Chen, *Biomicrofluidics*, 2013, **7**, 011801.
149 N. Tottori, T. Nisisako, J. Park, Y. Yanagida and T. Hatsuzawa, *Biomicrofluidics*, 2016, **10**, 014125.
150 S. H. Holm, J. P. Beech, M. P. Barrett and J. O. Tegenfeldt, *Lab Chip*, 2011, **11**, 1326–1332.
151 S. Ranjan, K. K. Zeming, R. Jureen, D. Fisher and Y. Zhang, *Lab Chip*, 2014, **14**, 4250–4262.
152 L. R. Huang, E. C. Cox, R. H. Austin and J. C. Sturm, *Science*, 2004, **304**, 987–990.
153 D. W. Inglis, J. A. Davis, R. H. Austin and J. C. Sturm, *Lab Chip*, 2006, **6**, 655–658.
154 K. Loutherback, K. Chou, J. Newman, J. Puchalla, R. Austin and J. Sturm, *Microfluid. Nanofluid.*, 2010, **9**, 1143–1149.
155 K. K. Zeming, T. Salafi, C.-H. Chen and Y. Zhang, *Sci. Rep.*, 2016, **6**, 22934.
156 S. M. Santana, M. A. Antonyak, R. A. Cerione and B. J. Kirby, *Biomed. Microdevices*, 2014, **16**, 869–877.
157 J. C. Sturm, E. C. Cox, B. Comella and R. H. Austin, *Interface Focus*, 2014, **4**, 20140054.
158 H. N. Joensson, M. Uhlén and H. A. Svahn, *Lab Chip*, 2011, **11**, 1305–1310.
159 X. Chen, D. Cui and J. Chen, *Electrophoresis*, 2009, **30**, 3168–3173.
160 L. Amato, Y. Gu, N. Bellini, S. M. Eaton, G. Cerullo and R. Osellame, *Lab Chip*, 2012, **12**, 1135–1142.
161 E. Ban, Y. S. Yoo and E. J. Song, *Talanta*, 2015, **141**, 15–20.
162 A. A. S. Bhagat, S. S. Kuntaegowdanahalli, D. D. Dionysiou and I. Papautsky, *MOEMS-MEMS 2008 Micro and Nanofabrication*, 2008, pp. 688600–688611.
163 J. Regtmeier, J. Käsewieter, M. Everwand and D. Anselmetti, *J. Sep. Sci.*, 2011, **34**, 1180–1183.
164 S. Suh, M. A. Traore and B. Behkam, *Lab Chip*, 2016, **16**, 1254–1260.
165 D. Li, *Electrokinetics in microfluidics*, Academic Press, 2004.
166 S. H. Donaldson Jr, S. Das, M. A. Gebbie, M. Rapp, L. C. Jones, Y. Roiter, P. H. Koenig, Y. Gizaw and J. N. Israelachvili, *ACS Nano*, 2013, **7**, 10094–10104.
167 M. Krishnan, N. Mojarad, P. Kukura and V. Sandoghdar, *Nature*, 2010, **467**, 692–695.
168 J. Wu, X. Wu and F. Lin, *Lab Chip*, 2013, **13**, 2484–2499.
169 M. A. Traore and B. Behkam, *J. Micromech. Microeng.*, 2013, **23**, 085014.
170 R. Ashton, C. Padala and R. S. Kane, *Curr. Opin. Biotechnol.*, 2003, **14**, 497–504.
171 N. Minc, C. Fütterer, K. D. Dorfman, A. Bancaud, C. Gosse, C. Goubault and J.-L. Viovy, *Anal. Chem.*, 2004, **76**, 3770–3776.
172 M. Viefhues, J. Regtmeier and D. Anselmetti, *Analyst*, 2013, **138**, 186–196.
173 R. H. Austin, *Electrophoresis*, 2002, **23**, 3496–3503.
174 Y. Chen, E. S. Abrams, T. C. Boles, J. N. Pedersen, H. Flyvbjerg, R. H. Austin and J. C. Sturm, *Phys. Rev. Lett.*, 2015, **114**, 198303.
175 J. Wen, J. Albrecht, E. W. Wilker, M. B. Yaffe and K. F. Jensen, *Proceedings of the 12th International Conference on Miniaturized Systems for Chemistry and Life Sciences (μTAS2008)*, pp. 492–495.
176 C. Herzog, E. Poehler, A. J. Peretzki, S. M. Borisov, D. Aigner, T. Mayr and S. Nagl, *Lab Chip*, 2016, **16**, 1565–1572.
177 H. Ding, X. Li, X. Lv, J. Xu, X. Sun, Z. Zhang, H. Wang and Y. Deng, *Analyst*, 2012, **137**, 4482–4489.
178 C. F. Ivory and S. K. Srivastava, *Electrophoresis*, 2011, **32**, 2323–2330.
179 D. Kim, J. Shim, H.-S. Chuang and K. C. Kim, *J. Mech. Sci. Technol.*, 2014, **28**, 2629–2636.
180 A. Nakano, F. Camacho-Alanis, T.-C. Chao and A. Ros, *Biomicrofluidics*, 2012, **6**, 034108.
181 E. Sollier and D. Di Carlo, *Microfluidic Technologies for Human Health*, 2012, p. 311.
182 T. R. Poloni, A. S. Oliveira, H. L. Alfonso, L. R. Galvão, A. A. Amarilla, D. F. Poloni, L. T. Figueiredo and V. H. Aquino, *Virol. J.*, 2010, **7**, 1.
183 A. Y. Yamamoto, M. M. Mussi-Pinhata, L. J. Marin, R. M. Brito, P. F. C. Oliveira and T. B. Coelho, *J. Clin. Virol.*, 2006, **36**, 228–230.
184 M. R. Karim, E. R. Rhodes, N. Brinkman, L. Wymer and G. S. Fout, *Appl. Environ. Microbiol.*, 2009, **75**, 2393–2399.
185 S. Wang, D. Sarenac, M. H. Chen, S.-H. Huang, F. F. Giguel, D. R. Kuritzkes and U. Demirci, *Int. J. Nanomed.*, 2012, **7**, 5019–5028.
186 E. J. Fong, A. C. Johnston, T. Notton, S.-Y. Jung, K. A. Rose, L. S. Weinberger and M. Shusteff, *Analyst*, 2014, **139**, 1192–1200.
187 S. A. Melo, H. Sugimoto, J. T. O'Connell, N. Kato, A. Villanueva, A. Vidal, L. Qiu, E. Vitkin, L. T. Perelman and C. A. Melo, *Cancer Cell*, 2014, **26**, 707–721.

188 S. Keller, J. Ridinger, A.-K. Rupp, J. W. Janssen and P. Altevogt, *J. Transl. Med.*, 2011, **9**, 86.
189 G. Raposo and W. Stoorvogel, *J. Cell Biol.*, 2013, **200**, 373–383.
190 M. He, J. Crow, M. Roth, Y. Zeng and A. K. Godwin, *Lab Chip*, 2014, **14**, 3773–3780.
191 R. J. Lobb, M. Becker, S. Wen Wen, C. S. F. Wong, A. P. Wiegmans, A. Leimgruber and A. Möller, *J. Extracell. Vesicles*, 2015, **4**, 27031.
192 A. H. Ng, K. Choi, R. P. Luoma, J. M. Robinson and A. R. Wheeler, *Anal. Chem.*, 2012, **84**, 8805–8812.
193 A. Liga, A. Vliegenthart, W. Oosthuyzen, J. Dear and M. Kersaudy-Kerhoas, *Lab Chip*, 2015, **15**, 2388–2394.
194 C. Théry, L. Zitvogel and S. Amigorena, *Nat. Rev. Immunol.*, 2002, **2**, 569–579.
195 Z. Zhao, Y. Yang, Y. Zeng and M. He, *Lab Chip*, 2016, 489–496.
196 R. Narayanan and M. A. El-Sayed, *Nano Lett.*, 2004, **4**, 1343–1348.
197 Y. Pan, S. Neuss, A. Leifert, M. Fischler, F. Wen, U. Simon, G. Schmid, W. Brandau and W. Jahnen-Dechent, *Small*, 2007, **3**, 1941–1949.
198 S. Dubascoux, F. Von Der Kammer, I. Le Hécho, M. P. Gautier and G. Lespes, *J. Chromatogr. A*, 2008, **1206**, 160–165.
199 L. A. Godwin, K. S. Deal, L. D. Hoepfner, L. A. Jackson and C. J. Easley, *Anal. Chim. Acta*, 2013, **758**, 101–107.
200 D. W. Inglis, M. Lord and R. E. Nordon, *J. Micromech. Microeng.*, 2011, **21**, 054024.
201 B. L. Khoo, M. E. Warkiani, D. S.-W. Tan, A. A. S. Bhagat, D. Irwin, D. P. Lau, A. S. Lim, K. H. Lim, S. S. Krisna and W.-T. Lim, *PLoS One*, 2014, **9**, e99409.
202 S. K. R. Williams, J. R. Runyon and A. A. Ashames, *Anal. Chem.*, 2010, **83**, 634–642.
203 J. D. Robertson, L. Rizzello, M. Avila-Olias, J. Gaitzsch, C. Contini, M. S. Magoń, S. A. Renshaw and G. Battaglia, *Sci. Rep.*, 2016, **6**, 27494.
204 M. T. Blom, E. Chmela, R. E. Oosterbroek, R. Tijssen and A. van den Berg, *Anal. Chem.*, 2003, **75**, 6761–6768.
205 H. Shintaku, H. Nishikii, L. A. Marshall, H. Kotera and J. G. Santiago, *Anal. Chem.*, 2014, **86**, 1953–1957.
206 D. G. Rackus, M. H. Shamsi and A. R. Wheeler, *Chem. Soc. Rev.*, 2015, **44**, 5320–5340.
207 A. Dawoud, T. Kawaguchi, Y. Markushin, M. D. Porter and R. Jankowiak, *Sens. Actuators, B*, 2006, **120**, 42–50.
208 A. D. Bani-Yaseen, T. Kawaguchi, A. K. Price, C. T. Culbertson and R. Jankowiak, *Anal. Bioanal. Chem.*, 2011, **399**, 519–524.
209 J. S. Mellors, W. A. Black, A. G. Chambers, J. A. Starkey, N. A. Lacher and J. M. Ramsey, *Anal. Chem.*, 2013, **85**, 4100–4106.
210 C. Wang, A. B. Jemere and D. J. Harrison, *Electrophoresis*, 2010, **31**, 3703–3710.
211 X. Wang, L. Yi, N. Mukhitov, A. M. Schrell, R. Dhumpa and M. G. Roper, *J. Chromatogr. A*, 2015, **1382**, 98–116.
212 D. Gao, H. Liu, Y. Jiang and J.-M. Lin, *Lab Chip*, 2013, **13**, 3309–3322.
213 V. Pospichalova, J. Svoboda, Z. Dave, A. Kotrbova, K. Kaiser, D. Klemova, L. Ilkovics, A. Hampl, I. Crha and E. Jandakova, *J. Extracell. Vesicles*, 2015, **4**, 25530.
214 H. Shao, J. Chung, L. Balaj, A. Charest, D. D. Bigner, B. S. Carter, F. H. Hochberg, X. O. Breakefield, R. Weissleder and H. Lee, *Nat. Med.*, 2012, **18**, 1835–1840.
215 Q. Wei, H. Qi, W. Luo, D. Tseng, S. J. Ki, Z. Wan, Z. N. Göröcs, L. A. Bentolila, T.-T. Wu and R. Sun, *ACS Nano*, 2013, **7**, 9147–9155.